eLife

Reviewed Preprint
v1 • February 12, 2026
Not revised

Reviewed Preprint
v2 • April 30, 2026
Revised by authors

Sexual dimorphism in sensorimotor transformation of optic flow

Sarah Nicholas[1], Katja Sporar Klinge[1,#], Luke Turnbull[1], Annabel Moran[1], Aika Young[1], Yuri Ogawa[1] ✉, Karin Nordström[1,2] ✉

[1]Flinders Health and Medical Research Institute, Flinders University, Adelaide, Australia • [2]Department of Medical Cell Biology, Uppsala University, Uppsala, Sweden

For correspondence:
yuri.ogawa@flinders.edu.au
karin.nordstrom@flinders.edu.au

[#] Current address: Institute for Developmental Biology, RWTH Aachen University, 52074 Aachen, Germany

Competing interests: No competing interests declared

Funding: See page 25

Reviewing editor: Albert Cardona, University of Cambridge, United Kingdom

eLife Assessment

Hoverflies are known for their sexually dimorphic visual systems and exquisite flight behaviors. This **valuable** study reports how two types of visual descending neurons differ between males and females in their motion- and speed-dependent responses, yet surprisingly, the behavior they control lacks any sexual dimorphism. The results **convincingly** support these findings, which will be of interest for studies of visuomotor transformations and network-level brain organization.

https://doi.org/10.7554/eLife.109795.2.sa3

Abstract

Motion vision underpins a wide range of adaptive behaviours essential for individual and species survival. In hoverflies, some visual behaviours are sexually dimorphic, including for example male high-speed pursuit of conspecifics, matched by improved optics, and faster photoreceptors. Other visual behaviours are sexually monomorphic, with for example similar foraging flight speeds in male and female hoverflies. However, whether the descending neurons responsible for sensorimotor transformation of optic flow are sexually dimorphic is unknown. To address this, we combined morphological analysis with electrophysiology of optic flow sensitive descending neurons and compared neural responses to the behavioural output in tethered hoverflies. We found that while optomotor flight behaviour is largely sexually monomorphic, the underlying neural responses are sexually dimorphic, especially at higher optic flow velocities. Additionally, behavioural responses were noticeably slower than neural responses. Together, our findings uncover a nuanced, sex- and stimulus- dependant sensorimotor transformation, shaped by both neural architecture and behavioural demands.

Introduction

Motion vision is a fundamental sensory modality across the animal kingdom, enabling animals to navigate, to maintain a straight trajectory, to avoid collisions, and to identify prey, predators or mates. Among the most potent cues for self-motion is widefield optic flow, the coherent motion of the entire visual field, generated by an animal's own movement through the world. In insects, the neural mechanisms underlying optic flow processing have been studied extensively (for a review, see e.g. Ref [1]), offering a powerful model for understanding how compact nervous systems extract behaviourally relevant information from dynamic visual scenes.

To generate appropriate responses to widefield optic flow, the visual input needs to be integrated across space. In flies, this spatial pooling occurs in 45-60 lobula plate tangential cells (LPTCs)[2,3], each matched to a particular type of self-generated optic flow[4], where the horizontal system (HS) and vertical system (VS) cells are the most well described. HS cells respond optimally to rotations around the yaw axis, whereas VS cells are tuned to pitch and roll rotations[5]. LPTCs project to the inferior posterior slope[6], where they synapse with descending neurons[7,8]. In *Drosophila* at least 35 descending neuron types have their inputs in the posterior surface of the brain (named DNp1-35)[9].

Furthermore, in *Drosophila* and blowflies, three of these descending neurons have been shown to respond robustly to widefield optic flow. Their axons project to the dorsal part of the thoracic ganglion, where motor neurons controlling the neck, wings and halteres are located[7,10–13].

DNp15, also called DNHS1, receives input from HS cells[9–11] and is physiologically similar to the optic flow sensitive descending neuron type 1 (OFS DN1) in the hoverfly *Eristalis tenax*[14], although direct LPTC coupling has not yet been demonstrated in the hoverfly.

DNHS1 projects to the neck and haltere motor neuropils[9] and has been implicated in the control of head yaw movements, abdominal ruddering and flight stabilization via the haltere motor system[10]. DNp20, or DNOVS1, receiving input from the ocelli and VS cells[7,9,10,15], is likely involved in rapid head movements[9], possibly facilitating gaze stabilization during flight[10]. DNp22, or DNOVS2, also receives input from the ocelli but a different subset of VS cells[7,9,10,16]. DNOVS2 is physiologically similar to the *Eristalis tenax* optic flow sensitive descending neuron type 2 (OFS DN2)[14], but synaptic coupling with VS cells has not been shown in hoverflies. DNOVS2 projects to the neck, wing and haltere motor neuropils[9] and has been implied in the initiation of the fast body saccades that support rapid re-orientation[10] during flight in response to dynamic visual cues.

Hoverflies are interesting in the context of motion vision, which they use both to maintain a hovering stance, and to fly at high speed[17]. Indeed, hoverflies show striking sexually dimorphic flight behaviour, where males establish territories which they guard rigorously from a hovering stance[18], followed by high-speed flight to chase away any intruding insects and/or pursue conspecific females for courtship and mating[17,19]. Male hoverflies are also smaller than females[20,21], which introduces an aerodynamic component by reducing inertia and enabling finer control over rapid flight adjustments[22]. Accompanying this sexually dimorphic pursuit behaviour, male *E. tenax* have larger lenses than females in a dorso-frontal bright zone[23], with faster motion detection and increased signal-to-noise ratio[24]. In many fly species, the photoreceptors in this part of the eye are also faster in males[25]. In hoverflies, even if the LPTCs are typically implied in optomotor responses[1], males have a smaller HSN receptive field[26] and velocity tuning shifted to higher velocities[23,27]. These adaptations are likely useful in regulating optomotor responses during high-speed target pursuit[28,29]. Indeed, as target selective descending neurons (TSDNs) are suppressed when target and background move in the same direction[28,30], the optic flow sensitive descending neurons may serve a complementary role in stabilizing flight under these conditions.

The differences in optics, photoreceptor dynamics, and LPTC receptive field size and velocity tuning, have been interpreted as required by males in the fast flight used during sexually dimorphic territorial behaviours. Interestingly, there is no sexual dimorphism in flight speed during behaviours likely to be governed primarily by the LPTCs, such as foraging between flowers[31] and when flying within the confines of an indoor arena[32]. To investigate the discrepancy between sexually dimorphic visual processing and sexually monomorphic flight speed, we compared the electrophysiological response characteristics and morphology of optic flow sensitive descending neurons in male and female hoverflies and linked these findings to the behaviour of tethered hoverflies viewing similar stimuli. We used the wing beat amplitude (WBA) as a measure of the optomotor response, and found no sexual dimorphism at speeds up to 2 m/s for translation and 200°/s for rotation. While the head movements were largely sexually monomorphic, the extension of the fore- and hind legs exhibited clearer sexual dimorphism. Furthermore, while neural morphology, receptive fields and direction sensitivity of the descending neurons showed minimal sex differences, there was a significant and noticeable difference in the velocity response functions between males and females, especially at higher speeds. Critically, neural differences were not only velocity dependent but also varied between stimuli (occurring only for sideslip, lift and thrust, but not roll) and neuron type. These neuron-, stimulus-, and sex-specific differences uncovers a previously unrecognized complexity in the neural encoding of visual motion, revealing for the first time, a sex-dependent transformation from sensory input to motor output.

Results

Two distinct types of optic flow sensitive descending neurons can be identified by their receptive field location and preferred direction

Optic flow sensitive descending neurons can be readily identified by mapping their receptive field using small sinusoidal gratings[14,23]. Based on the receptive fields of 100 reference neurons recorded from 90 male hoverflies, we found that two key parameters, the azimuthal position of the receptive field centre and its preferred direction of motion, are sufficient to reliably ascertain neuron type (Fig. 1, Supplementary Fig. 1). OFS DN1 has a preferred direction up and away from the midline, either leftward (range from 137° to 171°) or rightward (range from 16° to 40°) for neurons on the left- and right-hand side of the visual field, respectively (Fig. 1a, b and c; green, Fig. 1g, h and i). OFS DN2 neurons respond preferentially to downward motion (range from 228° to 293°; Fig. 1d, e and f; yellow and orange, Fig. 1g, h and i) with the azimuthal position of the receptive field centre separating left-hand side (LHS) from right-hand side neurons (RHS, Fig. 1g, h and i).

We used the maximum local motion sensitivity (LMS, Fig. 1c, f), the extent of the receptive fields (number of positions with LMS over 50%, arrows in Fig. 1c, f) and the local preferred direction (LPD, Fig. 1c, f) variance from these 100 reference neurons (grey data, Supplementary Fig. 2a, b and c) to set strict exclusion criteria (dashed red, Supplementary Fig. 2a, b and c) of the neurons used in the rest of the paper. This resulted in the exclusion of two neurons from males and seven from females (grey, Supplementary Fig. 2d, e) due to either low LMS (less than 20 spikes/s, Supplementary Fig. 2a), a small number of locations where LMS exceeded 50% of the maximum (four positions or less, Supplementary Fig. 2b) or high LPD variance (above 30°, Supplementary Fig. 2c).

We found no sexual dimorphism in either neuron type when comparing receptive field width and height of the remaining 33 male and 29 female neurons (Supplementary Fig. 2f, unpaired t-test, p = 0.52 and 0.09 for width and height of OFS DN1, and p = 0.19 and 0.13 for width and height of OFS DN2).

Directional tuning of optic flow sensitive descending neurons exhibits limited sexual dimorphism

Some LPTCs, which are upstream of optic flow sensitive descending neurons, show distinct sexual dimorphism, whilst others do not[23,26]. The receptive field data used for classifying OFS DN1 and DN2 showed that they are strongly directional (Fig. 1g, i). To investigate if this direction tuning is sexually dimorphic, we used a separate experiment quantifying responses to full-screen sinusoidal grating stimuli (wavelength 7°, 5 Hz, Supplementary Fig. 3). We found that the resulting preferred direction of both OFS DN1 and OFS DN2 matched their receptive field preferred directions (compare polar plots in Supplementary Fig. 2d, e with Supplementary Fig. 3g, h), i.e. up and away from the visual midline for OFS DN1 (range from 359° to 52°) or downwards for OFS DN2 (range from 273° to 297°, Fig. 2a). Whilst OFS DN1 showed no difference in preferred direction between the sexes (Watson-Williams two-sample test, p = 0.38), male OFS DN2 had a slightly more lateral preferred direction compared to females (Fig. 2a; median = 285.4° compared to 281.5°, Watson-Williams two-sample test, p = 0.046).

We quantified the spontaneous rate and found that neither this nor the responses of OFS DN1 to a stationary starfield pattern differed between the sexes (circles, Supplementary Fig. 4a, two-way ANOVA, p = 0.29). Conversely, OFS DN2 exhibited significant sexual dimorphism, with females displaying a higher spontaneous rate and response to stationary stimuli than males (circles, Supplementary Fig. 4b, two-way ANOVA, p < 0.001). The response to a stationary stimulus was larger than spontaneous rate in males (p = 0.015), but not in females (red circles, Supplementary Fig. 4b, p = 0.35, two-way ANOVA).

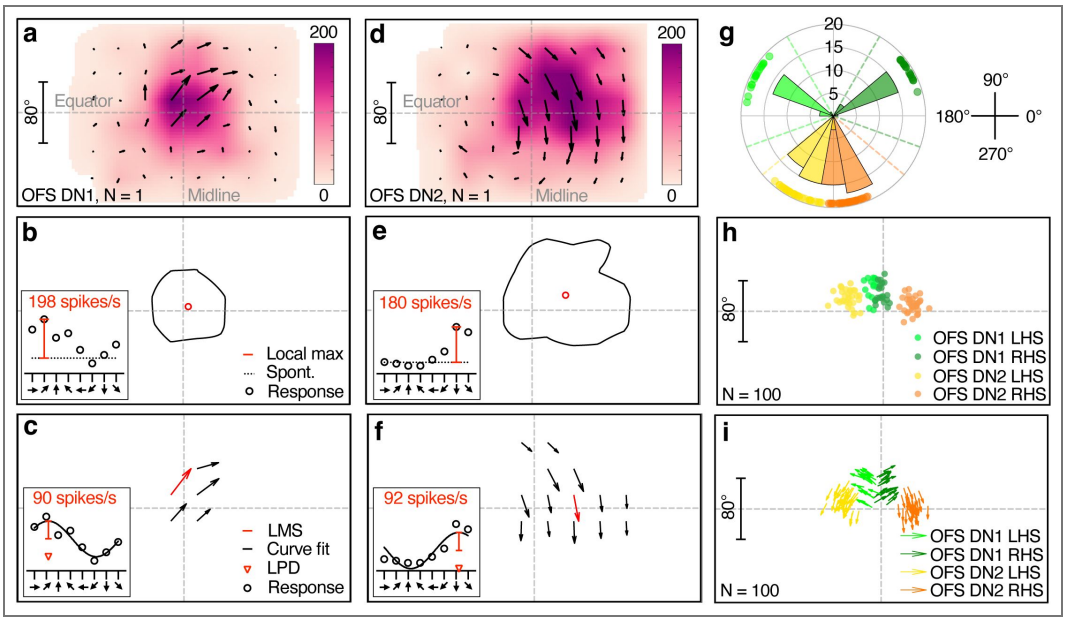

Fig. 1. Classification of optic flow sensitive (OFS) descending neurons (DN) in *Eristalis tenax*.

a Receptive field of a representative OFS DN1 recorded from a male hoverfly. Colour coding indicates the local maximum spike frequency (red, inset, panel b), the direction of the arrows shows the local preferred direction (LPD, red arrowhead, panel c) and their length the local motion sensitivity (LMS, red, panel c). As the stimuli were not perspective corrected, the receptive field map reflects the visual monitor. **b** Contour line representing the 50% receptive field boundary based on local maximum spike frequency (colour coding, panel a). Inset: example response at one central location to eight directions of motion (black circles), showing local maximum spike frequency (local max, red line) above spontaneous rate (spont, black dotted line). **c** Local preferred direction (LPD) map of the same example neuron at locations where local motion sensitivity (LMS) exceeds 50% of the maximum. Inset: example response at one location to eight directions of motion with a sinusoidal fit (black line), illustrating LMS (red line) and LPD (red arrowhead). The data in the inset corresponds to the red arrow. **d** Receptive field of a representative male OFS DN2. **e** 50% receptive field contour and receptive field centre of the neuron shown in panel d. **f** Preferred direction map of the same OFS DN2. **g** Distribution of receptive field preferred directions across 100 male reference neurons, colour-coded by neuron classification. Dashed lines in corresponding colours indicate the thresholds used for neuron type classification. **h** Receptive field centres of the same 100 reference neurons, using the same colour coding. **i** Relationship between preferred direction and receptive field centre for the 100 neurons. Note that the scale is the same for the azimuth and elevation, and the scale bar in panels a, d, h and i correspond to both the x- and y-axis.

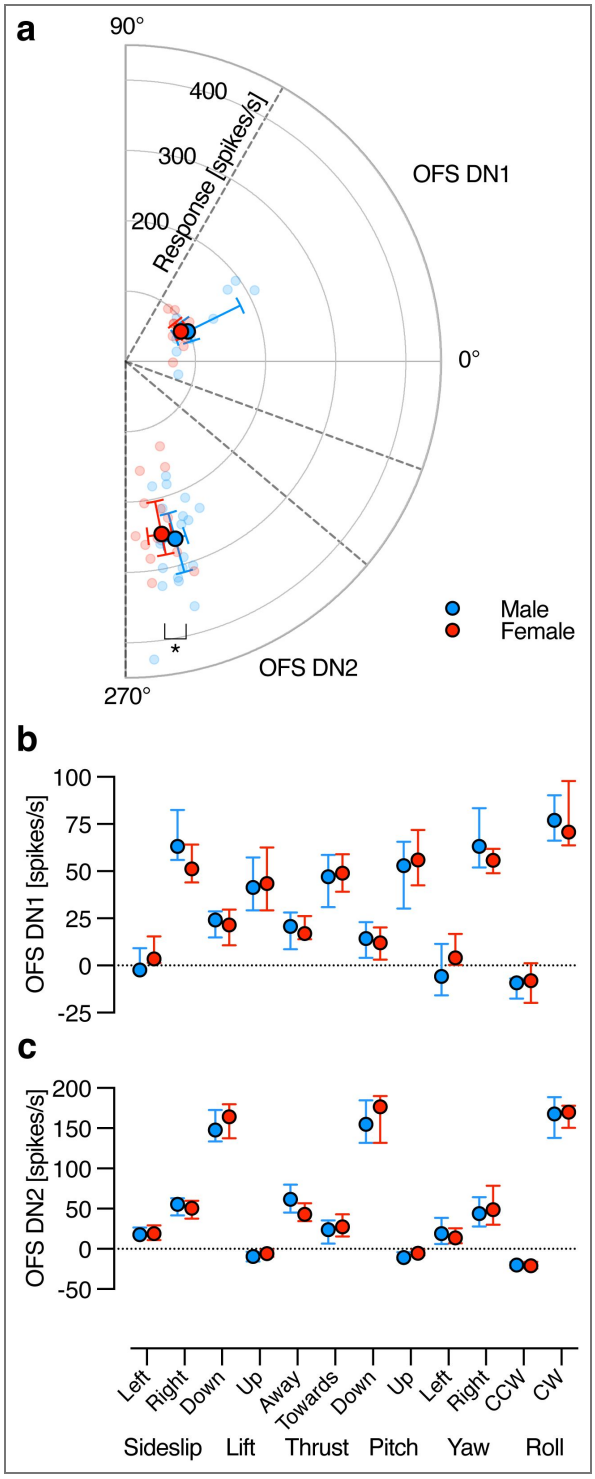

Fig. 2. Sex-based comparison of direction sensitivity in OFS DNs.

a Polar plot showing the preferred direction of male (blue) and female (red) OFS DNs in response to a full-screen, full-contrast sinusoidal grating (spatial wavelength 7°, temporal frequency 5 Hz) moving in eight different directions (see also Supplementary Fig. 3). Individual data points represent the response amplitude and preferred direction of each OFS DN (red, Supplementary Fig. 3j). Larger, salient circles indicate the population median, with error bars showing the interquartile range. The dashed lines indicate the directional thresholds used to classify neuron type, as OFS DN1 (male: N = 9; female: N = 12) or OFS DN2 (male: N = 20; female: N = 14). Asterisk indicates a statistically significant difference ($p < 0.05$, Watson-Williams two-sample test). **b** Comparison of male and female OFS DN1 responses to translational optic flow at 0.5 m/s: sideslip, lift and thrust; and rotational optic flow at 50 °/s: pitch, yaw and roll (male: N = 9; female: N = 12). **c** Comparison of male and female OFS DN2 responses to the same optic flow stimuli (male: N = 20; female: N = 14). Data presented as median and interquartile range.

We next looked at the responses to moving full-screen 3-dimensional starfield stimuli simulating the type of optic flow that would be generated by self-motion through space[33] (at 0.5 m/s for translations and 50°/s for rotations), after subtracting the response to the stationary stimulus (filled circles, Supplementary Fig. 4a, b). As predicted from the receptive fields (Fig. 1) OFS DN1 was excited by stimuli moving either up or away from the midline, such as rightward sideslip and yaw, and upwards lift and pitch (Fig. 2b), whilst OFS DN2 showed the strongest responses to downwards lift and pitch (Fig. 2c). Both neuron types respond strongly to clockwise roll (Fig. 2b, c), as predicted by their receptive fields (Fig. 1a, b) and shown previously for males[14]. However, neither neuron type showed any sexual dimorphism (Fig. 2b, c, two-way ANOVA, p = 0.81 and 0.92, OFS DN1 and OFS DN2, respectively).

Sexual dimorphism in optic flow descending neurons is velocity dependent

As the velocity tuning of some LPTCs is sexually dimorphic[23,27], we tested the responses of optic flow sensitive descending neurons using a continuous velocity step stimulus (Fig. 3, Supplementary movie 1). Six velocities for each direction of the stimuli (e.g. anticlockwise roll -10 to -200°/s and clockwise roll +10 to +200°/s) and a stationary control were presented three times each in random order for 2 s each (see example, Fig. 3a).

We confirmed that the spontaneous rate and response to stationary stimuli was significantly higher in females compared to males for OFS DN2 but not for OFS DN1 (triangles, Supplementary Fig. 4a, b, two-way ANOVA, p = 0.18 and $p < 0.001$, OFS DN1 and OFS DN2, respectively). As above, we subtracted the average response to the stationary stimulus from the responses to moving optic flow. The resulting data show that both neuron types exhibit sexual dimorphism to certain types of optic flow (Fig. 3e, f and Table 1). For example, the OFS DN1 response to thrust show a significant interaction between sex and velocity, with female neurons responding stronger to positive thrust compared to males (Fig. 3e and Table 1). The OFS DN2 response to sideslip was significantly different between males and females, and there was a significant interaction between sex and velocity in the responses to sideslip, lift, and thrust, with males responding stronger to sideslip, lift and thrust (Fig. 3f and Table 1).

Morphological reconstruction suggests optic flow sensitive descending neurons could control the wings

By recording from the descending neurons intracellularly we could iontophoretically fill them with 3% neurobiotin following identification based on receptive field (as in Fig. 1). We found that OFS DN1 and OFS DN2 of either sex receive their input in the part of the brain where LPTCs have their output (Fig. 4a, b, d, e and f). Both neuron types project along the length of the thoracic ganglion, with several fine branches along the way (Fig. 4a, b, c, g, h and i), like *Drosophila* DNHS1 and DNOVS2[34]. In *Drosophila*, DNOVS2 projects more medially than DNHS1, which also has a more distal projection, close to the haltere nerve (HN)[34]. However, we saw no such differences between the projections of OFS DN1 and DN2 (Fig. 4a, b, c, g, h and i). In addition, both hoverfly neuron types have prominent outputs where the prothoracic and pterothoracic nerves likely get their inputs (T1 LN and PtN, Fig. 4a, b, c, g, h and i), which is more similar to the outputs of *Drosophila* DNOVS1[34]. These outputs suggest that OFS DN1 and DN2 could contribute to controlling the neck, wings and/or the forelegs.

Whilst there was no indication of extensive sexual dimorphism in the structural morphology of these neurons, OFS DN2 appears to be slightly wider along the length of the cervical connective in females (Supplementary Fig. 5a, b). In part, this may be due to female hoverflies being bigger[20,21] and therefore having a wider cervical connective (Supplementary Fig. 5c).

Fig. 3. Velocity response functions in male and female OFS DNs.

a Example stimulus profile over time, with roll velocity on the y-axis. **b** Representative spike histogram from a single trial from a male OFS DN2, smoothed using a 100 ms square-wave filter with 0.025 ms resolution, and time-aligned to the stimulus shown in panel a. Grey shading in panels a and b highlight the analysis windows used to calculate response. **c** Example extracellular raw data traces extracted from the analysis windows in panel b, illustrating neuronal responses to roll velocities of –150, 10, and 200 °/s. **d** Average spike frequency (grey circles) was calculated for each repetition from each neuron (N = 1 neuron, n = 18 repetitions), and the median of these (black) was used for further analysis. **e** Velocity response functions of OFS DN1 in male (blue) and female (red) hoverflies in response to roll (N = 4 males, 5 females), sideslip (N = 5, 6), lift (N = 4, 4), and thrust (N = 3, 5). **f** Velocity response functions of OFS DN2 to roll (N = 10 males, 8 females), sideslip (N = 6, 7), lift (N = 6, 7), and thrust (N = 6, 7). Data in panels e and f are presented as median and interquartile range. Asterisks indicate statistically significant differences, two-way ANOVA with Šídák's multiple comparisons test (** p < 0.01 and **** p < 0.0001), see also Table 1.

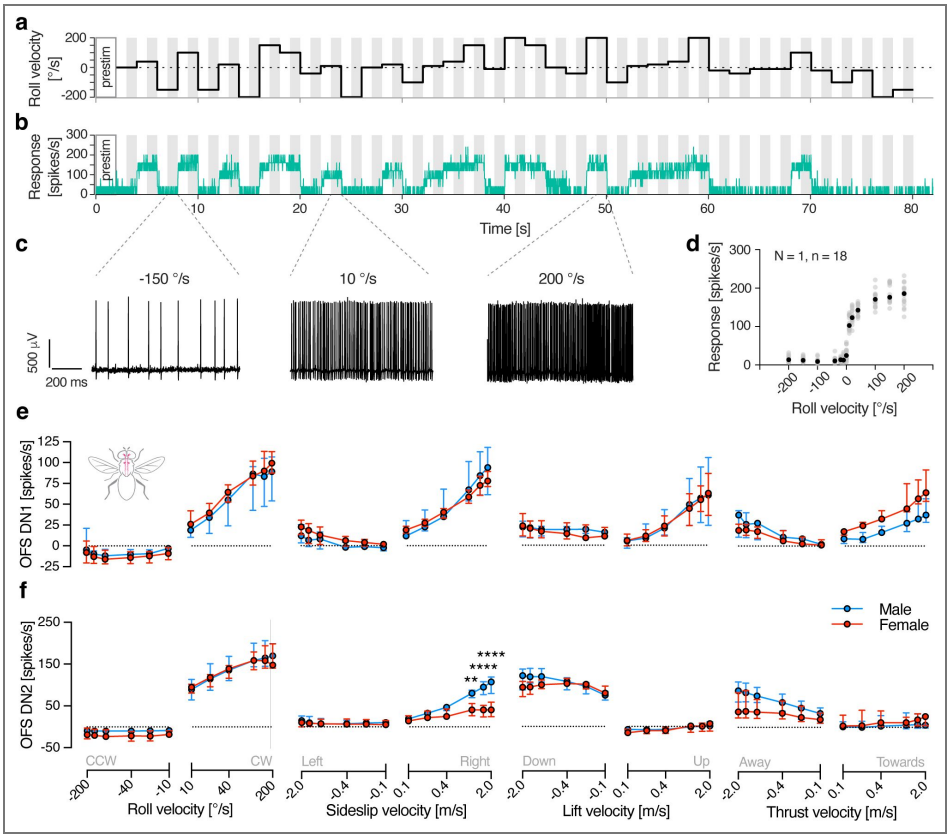

Table 1. Statistical summary of neural velocity response functions.

Results from two-way ANOVA analyses evaluating the effects of stimulus velocity and sex on neural responses (OFS DN1 and DN2). Asterisks denote levels of statistical significance: *** $p < 0.001$, **** $p < 0.0001$.

Stimulus		Velocity	Sex	Interaction		Velocity	Sex	Interaction
Roll	OFS DN1	****	0.35	0.14	OFS DN2	****	0.31	>0.99
Sideslip		****	0.90	0.12		****	**0.01**	****
Lift		**0.002**	0.86	>0.99		****	0.18	***
Thrust		****	0.11	****		****	0.10	**0.02**

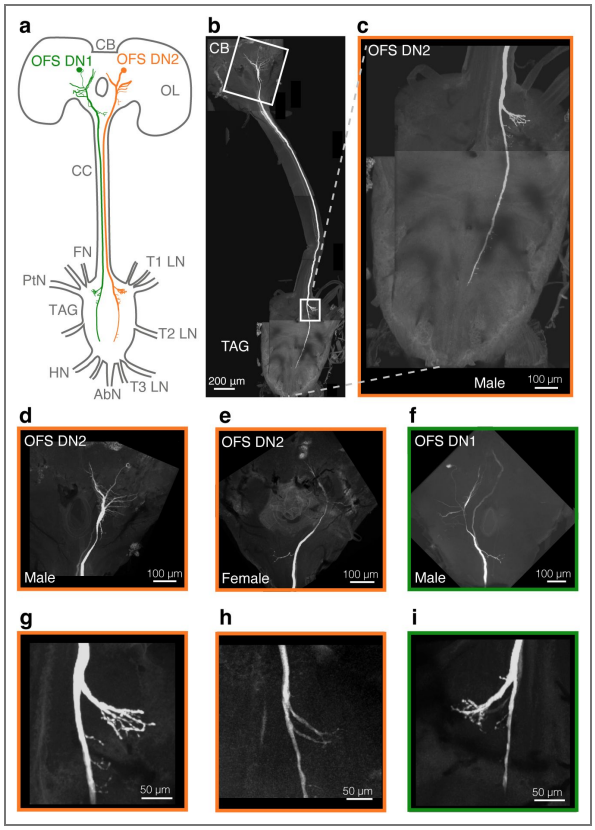

Fig. 4. Morphological reconstruction of OFS DNs.

a Schematic diagram of the hoverfly central brain and thoracic ganglia showing the projections of OFS DN1 (green) and OFS DN2 (orange). Key anatomical landmarks are labelled: CB, central brain; OL, optic lobe; CC, cervical connective; T1 LN, prothoracic leg nerve; T2 LN, mesothoracic leg nerve; T3 LN, metathoracic leg nerve; TAG, thoracic-abdominal ganglion; FN, frontal nerve; PtN, pterothoracic nerve; HN, haltere nerve; AbN, abdominal nerve. **b** Confocal image of a reconstructed male OFS DN2. White boxes indicate regions magnified in panels d - i. **c** A magnification of the thoracic ganglion in panel b. **d** Input dendrites of the same OFS DN2 around the sub-oesophageal ganglion. **e** Input dendrites of a female OFS DN2. **f** Input dendrites of a male OFS DN1. **g** Output projections of the same OFS DN2 neuron as in panels b, c and d. **f** Output projections within the thoracic ganglia of the neuron in panel e. **h** Output projections of the neuron in panel f.

Wing beat amplitude changes are velocity dependent but not sexually dimorphic

Given that the morphological data suggest that both neuron types could control the wings (Fig. 4), we conducted behavioural experiments in an open-loop tethered flight arena using the same continuous velocity stimulus as in electrophysiology (see Fig. 3a). We tracked the wing beat amplitude (WBA) for each wing (Fig. 5a, b, Supplementary movie 2) using DeepLabCut models[35,36] while the tethered animal was viewing different starfield velocities (Fig. 5c, d, e and f). Changes in the sum of the left and right WBA (WBAS, Fig. 5b) reflect variations in flight force generation, potentially contributing to either lift or thrust, while the difference between left and right WBA (WBAD) indicates yaw turning behaviour[37–39] or adjustments to body orientation[40].

The male WBAS is higher when viewing stationary stimuli compared with pre-stimulation ("pre stim" in Fig. 5c, d; blue, Supplementary Fig. 4c, two-way ANOVA followed by Uncorrected Fisher's LSD test, $p < 0.01$). However, there was no sexual dimorphism in the WBAS during pre-stimulation, nor when viewing stationary stimuli (Supplementary Fig. 4c, two-way ANOVA, $p = 0.35$). When comparing responses to each type of optic flow, after subtracting the response to stationary stimuli, both the WBAD and WBAS depended strongly on velocity, however, there was no sexual dimorphism (Fig. 5g, h and Table 2).

The lack of sexual dimorphism observed in behaviour (Fig. 5g, h and Table 2) contrasts with the neural responses (Fig. 3e, f and Table 1). Additionally, it is difficult to align the WBA responses to different types of optic flow with the neuronal input. For example, in response to higher clockwise roll velocities of (100 - 200°/s), hoverflies exhibit a decreased WBAD (positive roll, Fig. 5g) and a slightly increased WBAS (positive roll, Fig. 5h) indicating either a leftward turn or an anticlockwise body correction. Similarly, both RHS neuron types give strong responses to clockwise roll (positive roll, Fig. 3e, f). However, sideslip moving leftwards also elicits a decreased WBAD (negative sideslip, Fig. 5g) and an increased WBAS (negative sideslip, Fig. 5h) but neither neuron type responds strongly to this (negative sideslip, Fig. 3e, f).

We found that neither lift nor thrust evoke large turning responses (Fig. 5g), however, large and significant increases in the WBAS were observed in hoverflies experiencing the sensation of falling (positive lift, Fig. 5h and Table 2) or being pushed backwards (negative thrust, Fig. 5h and Table 2). Interestingly, each neuron type responds to lift and thrust in a different manner, with OFS DN1 being excited by upwards lift and approaching thrust (Fig. 3e), whereas OFS DN2 is excited by downwards lift and receding thrust (Fig. 3f).

In electrophysiology we used a horizontally oriented visual monitor (Supplementary Fig. 6a), whereas in behaviour the monitor was rotated 90° (Supplementary Fig. 6b and Ref [36]). To ensure that this did not substantially affect the shape of the velocity-response functions, we reduced the stimuli to the central square in both behaviour and electrophysiology. This reduction caused a slight but significant change in neuronal (central square; Supplementary Fig. 6c, two-way ANOVA, $p = 0.04$) and WBAS responses (central square; Supplementary Fig. 6d, two-way ANOVA, $p = 0.04$). However, it did not alter the shape of the velocity response function nor produce a significant interaction between velocity and screen size (two-way ANOVA, $p = 0.36$ and 0.49, OFS DN2 and WBAS, respectively).

Response onset depends on stimulus type

It has been previously shown that while neuronal responses are fast[33] behavioural responses occur on a much slower time scale and differ depending on stimulus type[41,42]. We here found that there is no significant effect of sex on either neuronal or WBAS response onset (Fig. 6, two-way ANOVA, $p = 0.21$, 0.79 and 0.31, OFS DN1, OFS DN2 and WBAS, respectively). However, the onset for roll compared to lift is significantly longer for OFS DN2 and WBAS but not for OFS DN1 (Fig. 6, two-way ANOVA, $p < 0.0001$ for both OFS DN2 and WBAS compared to $p = 0.08$ for OFS DN1). Note that we recorded the WBA from above (Fig. 5a), and as such did not quantify wing rotations and adjustments outside of the horizontal plane. The WBA response onset to roll optic flow (Fig. 6c) should thus be viewed as highly conservative.

Fig. 5. WBA velocity response functions in male and female hoverflies.

a A single frame from a video labelled with trained DeepLabCut models[35,36,55]. Coloured dots correspond to those in panel b, used to extract the wing beat amplitude (WBA). **b** Pictogram illustrating a higher wing beat amplitude on the left wing (WBA_L) compared to the right wing (WBA_R), suggesting a turn to the right. Equations used to calculate wing beat amplitude difference (WBAD) and wing beat amplitude sum (WBAS). **c** Example stimulus with sideslip velocity on the y-axis. **d** Representative WBA for the left (pale colour) and right (salient colour) wings from a single trial, time-aligned with the stimulus shown in panel c. Grey shading in panels c and d indicate the analysis windows used to calculate WBAD and WBAS. **e** Magnified view of example WBA, showing behavioural responses to sideslip velocities of -2, 0.2, and 2 m/s. **f** Average WBAS (grey circles) calculated across repetitions (N = 1 animal, n = 19-36 repetitions). Black circles represent the median WBAS per stimulus velocity, used for further analysis. **g** WBAD in male (blue) and female (red) hoverflies in response to different optic flow velocities: roll (N = 5 males, 7 females), sideslip (N = 6, 6), lift (N = 7, 5), and thrust (N = 6, 5). **h** WBAS to the same stimuli in the same animals. Data in panels g and h are presented as median and interquartile range.

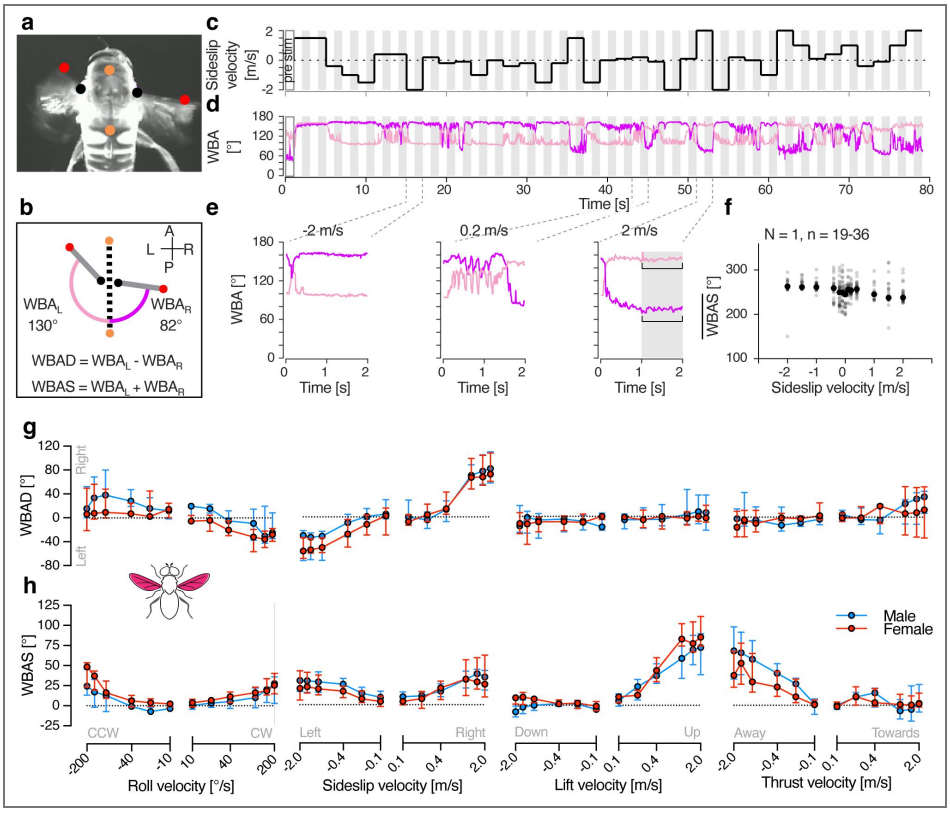

Table 2. Statistical summary of behavioural velocity response functions.

Results from two-way ANOVA analyses evaluating the effects of stimulus velocity and sex on behavioural responses (WBAS, WBAD, head angle, foreleg extension, hind leg extension and hind leg difference). Asterisks denote levels of statistical significance: ** $p < 0.01$, *** $p < 0.001$, **** $p < 0.0001$, after performing a Bonferroni correction[54] for 6 comparisons of data from the same videos.

Stimulus		Velocity	Sex	Interaction		Velocity	Sex	Interaction
Roll	WBAD	****	0.66	>0.99	WBAS	****	0.78	>0.99
Sideslip		****	>0.99	>0.99		****	>0.99	>0.99
Lift		0.18	>0.99	>0.99		****	0.54	0.12
Thrust		>0.99	>0.99	>0.99		**	>0.99	>0.99
Roll	Head	0.94	>0.99	>0.99	Foreleg	0.89	>0.99	0.26
Sideslip		**	>0.99	>0.99		**	**0.04**	**0.01**
Lift		>0.99	>0.99	>0.99		****	0.38	**0.03**
Thrust		>0.99	>0.99	0.08		**	>0.99	>0.99
Roll	Hind leg	0.21	>0.99	0.17	Δ Hind leg	**	>0.99	**0.02**
Sideslip		**0.04**	>0.99	**0.02**		****	>0.99	>0.99
Lift		0.39	>0.99	>0.99		0.41	>0.99	>0.99
Thrust		0.07	>0.99	>0.99		**	0.06	****

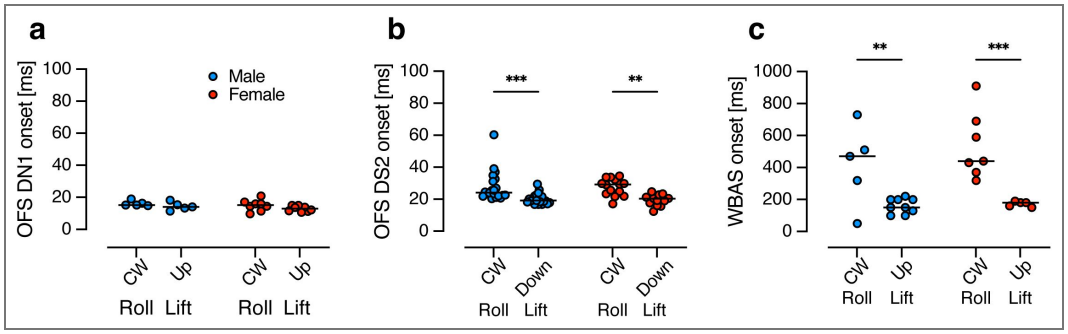

Fig. 6. Response onset to roll and lift stimuli in male and female hoverflies.

a Time to response onset in OFS DN1 to roll (+50 °/s) or lift (+0.5 m/s) stimuli in males (blue, N = 5) and females (red, N = 8). **b** Response onset in OFS DN2 to roll (+50 °/s) or lift (-0.5 m/s) measured in males (N = 20) and females (N = 14). **c** Onset of WBAS responses to roll (-200 °/s) and lift (+2 m/s) in males (N = 5 for roll, 9 for lift) and females (N = 7 for roll, 5 for lift). Data are presented from individual neurons (a, b) or animals (c) with lines indicating median. Asterisks indicate statistically significant differences, two-way ANOVA with uncorrected Fisher's LSD test (** $p < 0.01$ and *** $p < 0.001$).

Sideslip and lift optic flow generate strong head, fore- and hind leg movements

The lack of sexual dimorphism in WBA suggests that behavioural responses to optic flow are the same between the sexes. To investigate this further, we next extracted the head angle (Fig. 7a, b), and the extension of the fore- (Fig. 7a, c) and hind legs (Fig. 7a, d). We found that the head turned significantly when viewing sideslip (Supplementary movie 2 and 3, Fig. 7e and Table 2, two-way ANOVA, $p < 0.001$ for velocity), but there was no response to the other three types of optic flow. We found no sexual dimorphism (Fig. 7e and Table 2).

We found that while the forelegs could not be seen in the dorsal view for most of the flight (see e.g. Fig. 5a), they extended anteriorly in response to high velocity sideslip, lift and thrust, but not to roll (Fig. 7f , Table 2 and Supplementary movie 2-9). The foreleg extension to sideslip was sexually dimorphic, with significant interaction between sex and velocity for sideslip and lift motions (Fig. 7f and Table 2, two-way ANOVA, $p = 0.04, 0.01, 0.03$, respectively). Post hoc pairwise comparisons revealed females extended their forelegs further than males to upwards lift at 1.5 m/s (Fig. 7f, Šídák's multiple comparisons test, $p = 0.01$).

The hind legs were generally extended during flight (Fig. 5a, Fig. 7a) with males extending their legs further than females (Supplementary Fig. 4d, two-way ANOVA, $p = 0.032$). After subtracting the hind leg extension when viewing the stationary starfield (filled symbols, Supplementary Fig. 4d), we found similar patterns to foreleg extension (Fig. 7f), with a significant interaction between sex and velocity only in response to sideslip (Fig. 7g and Table 2, two-way ANOVA, $p = 0.02$). We quantified the difference between the right and the left hind leg and found that there was a significant interaction between sex and velocity in response to roll and thrust (Fig. 7h and Table 2, two-way ANOVA, $p = 0.02$ for roll and $p < 0.0001$ for thrust).

Looking at the different body parts together we noted that in response to upwards lift (generating a falling sensation) the WBAS increases substantially (Fig. 5h), and the fore-(Fig. 7f) and hind legs (Fig. 7g) all extend, potentially to brace for impact (Supplementary movie 4 and 5). We also noted that in response to sideslip, the WBAS increases (Fig. 5h), the WBAD indicates a turn in the direction of the optic flow (Fig. 5g), the head rotates (Fig. 7e), and both the forelegs and hind legs extend (Fig. 7f, g). The hind legs appear to be ruddering, with the right leg extending more when the animal is turning right (Fig. 5g, 7h, Supplementary movie 2 and 3). There was no significant difference in the response onset of these body parts, nor was there any sexual dimorphism (Supplementary Fig. 7).

Discussion

In the hoverfly, the optics, photoreceptors, and HS cells exhibit clear sexual dimorphism[23,24,26,27]. In line with this, our findings reveal that optic flow sensitive descending neurons also show sexually dimorphic velocity response functions (Fig. 3). Yet, despite the multi-level anatomical and neural sexual dimorphism, the wing beat amplitude (Fig. 5) and head movements (Fig. 7) remain mostly monomorphic, while leg movements exhibit clear sex-specific differences. Moreover, differences between neural and behavioural velocity response functions (Fig. 3, 5, 7) and response latency (Fig. 6) highlight the likely involvement of downstream processing mechanisms that could reconcile sex-specific sensory encoding with conserved flight control.

Some hoverfly flight behaviours are strongly sexually dimorphic, such as those related to courtship and mating. For example, male hoverflies defend territories from a hovering stance from which they pursue and capture female conspecifics at high speeds[19]. In contrast, other behaviours, including cruising speeds in field[31] and indoor settings[32] do not differ between sexes, and are much slower (median around 0.3 m/s[31,32]) than the 10 m/s that can be reached during outdoor pursuit[19]. In comparison, our results show limited sex-related differences in WBA in response to optic flow speeds up to 2 m/s (Fig. 5), yet we detected pronounced sexual dimorphism in neural responses at velocities as low as 0.5 m/s (Fig. 3, Table 1). This suggests that sensory processing differences emerge at lower velocities than the velocities where motor output diverges. Moreover, the WBAS response latencies were much longer than the

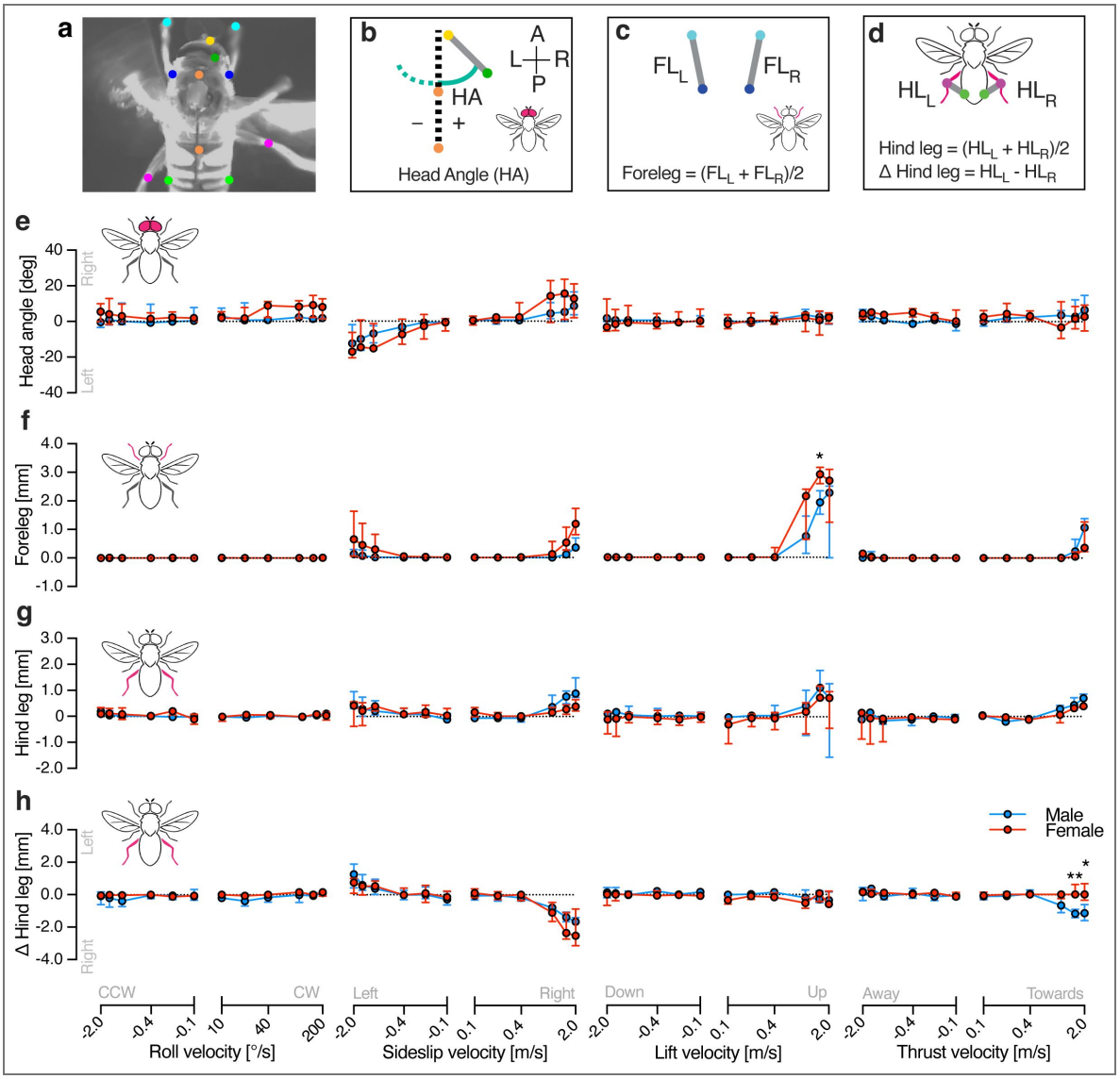

Fig. 7. Velocity response functions of the head, fore- and hind legs in male and female hoverflies.

a A single frame highlighting the points used to track the head (yellow and dark green), thorax (orange), forelegs (pale and dark blue), and hind legs (magenta and pale green). **b** The head angle (HA) was defined as the angle between the medio-posterior head and the longitudinal thorax axis. **c** The foreleg extension was defined as the distance between the proximal and distal point, after calculating the average for the left and the right leg. **d** The hind leg extension was defined as the distance between the knee and a lateral point on the mid-abdomen, after calculating the average for the left and the right leg. We also calculated the difference between the right and the left hind leg. **e** The head angle in male (blue) and female (red) hoverflies in response to different optic flow velocities: roll (N = 5 males, 7 females), sideslip (N = 6, 6), lift (N = 7, 5), and thrust (N = 6, 5). **f** The foreleg extension to the same stimuli in the same animals. **g** The hind leg extension in the same animals. **h** The difference between the left and right hind leg extension in the same animals. The data in panels e, f, g and h are presented as median and interquartile range. Asterisks indicate statistically significant differences, two-way ANOVA with Šídák's multiple comparisons test (* $p < 0.05$, ** $p < 0.01$), see also Table 2.

corresponding neural activity (Fig. 6), implying that temporal integration or additional circuit-level modulation may delay and refine motor execution. Together, these findings suggest a complex transformation between sex-specific sensory encoding and conserved motor behaviour, potentially mediated by downstream integration or additional alternate neural pathways that bypass the descending neurons studied here.

In *Drosophila* there are around 1000 descending neurons, of which at least 35 types receive their input in the posterior surface of the brain, which includes the inferior posterior slope, where the LPTC outputs are found[6,7,9]. However, only a subset of these constitute the 29 descending neuron types that project to the wing motor neuropil[9]. It is thus likely that the WBA that we recorded here (Fig. 5) reflects contributions from descending neurons beyond the two that we have characterised (Fig. 1, 3) in this study. For example, many looming sensitive neurons also respond to widefield optic flow[14,43] and could therefore play a role in the WBA changes that we detected (Fig. 5). While the morphology of both neurons (Fig. 4) suggested involvement in wing motor control, there is currently no direct evidence implicating them in the control of wingbeat amplitude. Interestingly, DNOVS2 in *Drosophila*, a physiologically similar neuron to OFS DN2[14], has been indirectly linked to rapid turning behaviour[10]. Furthermore, silencing HS and VS cells, the presumed presynaptic LPTCs to these descending neurons, results in reductions in WBA only at higher stimulus speeds[44]. These findings suggest that HS and VS cells, along with their downstream targets, may be specialized for driving fast optomotor responses under high-speed visual motion (>180°/s), rather than broadly regulating WBA across all velocities, including those examined in this study.

Beyond their potential involvement in wingbeat amplitude modulation, OFS DNs may play a role in coordinating head and body positioning during flight, especially in contexts requiring precise visual alignment and rapid manoeuvring. Indeed, the *Drosophila* physiological homologs of OFS DN1 and OFS DN2[14], DNHS1 and DNOVS2, project to the neck motor neuropil[9], and have been implicated in controlling head movements, abdominal ruddering, and engagement with the haltere motor system for flight stabilization[10]. While we did not quantify abdominal or haltere movements, we found that the head turned when viewing sideslip optic flow (Fig. 7e), and that the velocity dependence was similar to neural (Fig. 3e) and WBAD (Fig. 5g) responses. While we did not detect any head movements to roll, lift or thrust, this could be a technical limitation of recording from above (Fig. 5a). Indeed, many of the 29 descending neuron types that project to the wing motor neuropil, also project to the neck motor neuropil[9], suggesting that synchronized responses are not unexpected. Neither are the similar responses of the fore- and hind legs surprising (Fig. 7, f and g), considering that in *Drosophila* many of the ~30 descending neuron types that project to the forelegs, also project to the mid- and hind legs[9].

Our WBA recordings would also be affected by filming from above and thus lacking other nuanced changes in wing angles. Thus, the sexual dimorphism in neural responses (Fig. 3) could reflect an evolutionary tuning of visuomotor pathways in males, optimized for fast, directional adjustments rather than gross changes in WBA in the horizontal plane. For instance, whilst changes in WBAS are similar when generating either lift or thrust (Fig. 5h), body pitch dynamically adjusts their ratio, driving behavioural variation[45]. Thus, OFS DNs may serve as integral components of a broader flight control architecture, interfacing optic flow detection with dynamic body and head positioning systems to support complex, sex-specific behavioural outcomes, particularly in males engaging in high-speed pursuits.

Indeed, flight speed in insects results from a complex integration of multiple kinematic parameters, not solely from changes in wingbeat amplitude. Many species refine their aerodynamic output by modulating wingbeat frequency, angle of attack, wing tip trajectory, deviations from the mean stroke plane and through precise adjustments to the timing and duration of the up- and downstrokes[46]. These control strategies support agile manoeuvring, particularly during visually guided behaviours such as the high-speed pursuits undertaken by male hoverflies. Furthermore, the smaller body size of male hoverflies compared to females[20,21] may confer biomechanical advantages, including reduced mass, facilitating faster acceleration, heightened responsiveness, and lower metabolic costs for executing flight manoeuvres[22,47], which

do not appear in a tethered flight set-up. Such enhanced agility is likely crucial for rapid direction changes required during courtship and may enable male hoverflies to outperform female flies without relying on increased wingbeat amplitude.

Taken together, our findings reveal significant differences between sexually dimorphic sensory encoding and conserved motor output in hoverfly flight at cruising speeds. Although OFS DNs and their upstream visual circuits display clear sex-specific tuning, wingbeat amplitude and head angle changes in response to optic flow stimuli remain relatively similar between the sexes, suggesting additional mechanisms downstream of sensory input. This likely reflects a complex interplay of biomechanical properties, multisensory integration and circuit-level modulation, each shaping and refining behavioural outcomes to meet distinct demands, preserving the consistency of low-speed manoeuvres whilst enabling sex-specific tuning during high-speed pursuits.

Methods

Animals

For all experiments, male and female *Eristalis tenax* were reared and housed as described previously[21]. Briefly, eggs were collected from females captured under permit in Wittunga Botanic Garden, Adelaide, South Australia. Upon hatching, larvae were reared in a rabbit dung slurry until third instar larvae emerged to pupate. Eclosion occurred 1-2 weeks post-pupation. Adult hoverflies were used for behavioural experiments at 17-87 days post-eclosion, for intracellular electrophysiology and subsequent morphological reconstruction at 38-54 days, and for extracellular electrophysiology at 8-204 days.

Electrophysiology

Before recording the animal was immobilised, mounted dorsal side down (Supplementary Fig. 6a) and secured using a mixture of beeswax and resin. A small region of cuticle was removed at the anterior end of the thorax to expose the cervical connective. If required, any excessive gut or tracheal tissue obstructing the recording site was removed and a small volume of PBS was added to prevent drying within the ventral cavity. A fine wire hook was positioned under the cervical connective for mechanical support, and a silver wire was inserted into the cavity to serve as a reference electrode and grounding wire[14].

For extracellular recordings, a sharp tungsten microelectrode (2 MΩ, polyimide-insulated; Microprobes) was inserted into the cervical connective[14]. Signals were amplified 1000 times and band-pass filtered between 10–3000 Hz using a DAM50 differential amplifier (World Precision Instruments), followed by noise reduction with a HumBug (Quest Scientific). Data were digitized via a PowerLab 4/30 interface (ADInstruments) and acquired at 40 kHz. Spike sorting was performed in LabChart 7 Pro (ADInstruments) based on the amplitude and width of individual action potentials.

For intracellular recordings, aluminosilicate electrodes were pulled using a Sutter P-1000 micropipette puller, achieving a resistance of approximately 40-70 MO. Electrode tips were filled with 3% neurobiotin (Vector Laboratories), then backfilled with 1 M KCl using a syringe, leaving a small air bubble between the two solutions. Electrodes were inserted into the cervical connective for recording, and the resulting signal was amplified using an Axoclamp-2B amplifier (Axon Instruments), followed by 50 Hz noise reduction with a HumBug (Quest Scientific). Data acquisition and digitization were performed at 10 kHz using an NI USB-6210 16-bit data acquisition card (National Instruments) and the MATLAB Data Acquisition Toolbox (Mathworks), using in house software (*https://github.com/HoverflyLab/SampSamp*).

Morphological reconstructions

Following intracellular recordings, neurons were stained iontophoretically with neurobiotin using currents in the 1 nA range for 3–12 minutes. The nervous system was then carefully dissected and fixed in 4% paraformaldehyde overnight. Tissue was incubated with a Cy3-streptavidin conjugate (1:100; Jackson ImmunoResearch) for 2 hours, then dehydrated through an ethanol series (50–

100%) for 15-20 minutes per step. After washing in PBT, the tissue was cleared in RapiClear (SUNJIN Lab) and mounted with spacers. Imaging was performed using a Zeiss LSM 880 Fast Airyscan confocal microscope at the institutional microscopy facility. Neuron morphology and cervical connective width were quantified using ImageJ[48].

Tethered flight

Prior to flight recordings, hoverflies were tethered at a 32° angle (Supplementary Fig. 6b) using a beeswax–resin mixture to a small pin inserted into a hypodermic needle (BD Microlance, 23G × 1¼"). Flight was initiated by manually providing airflow for 1–10 minutes until consistent flight behaviour was observed. Once positioned facing the centre of the visual monitor (Supplementary Fig. 6b), hoverflies were filmed from above at 100 Hz using a Sony PlayStation 3 Move Eye Camera (SLEH- 00448, Sony) with the IR filter removed, and equipped with an infrared pass filter (R72 INFRARED, 49 mm, HOYA; for details see Ref[36]). Illumination was provided by infrared LEDs inserted into USB lights (JANSJÖ LED USB lamp, IKEA) and a Musou Black (Shin Kokushoku Musou black, KOYO Orient Japan) surface was placed beneath the hoverfly to enhance contrast and minimize optical interference.

We used DeepLabCut (DLC) version 2.3.3[35] to train a model to track the thorax, the peak downstroke angle, referred to as the wing beat amplitude (WBA), of the left and right wing (WBA_L and WBA_R; Fig. 5a, b), as described previously[36]. In addition, we tracked the dorso-medial head (yellow, green, Fig. 7a, b), the proximal and distal points of the forelegs (blue, Fig. 7a, c), the hind leg knee and the lateral, mid-abdomen (magenta, green, Fig. 7a, d). For this purpose, we first manually labelled the anatomical landmarks (Fig. 5a and Fig. 7a), across 16 extracted video frames per individual from four hoverflies (2 males, 2 females). In addition to examples where the hoverfly was not flying, these frames included responses to yaw rotation and forward translation. The DLC model was trained for 300,000 iterations, yielding train and test errors of 1.2 and 1.16 pixels, respectively.

To identify potential tracking errors from DLC, we smoothed the WBA time series using MATLAB's *smooth* function with both *loess* and *rloess* methods. Because *rloess* is more resistant to outliers, we used it to detect abnormal data points. For each wing, if the absolute difference between the *loess*- and *rloess*-smoothed signals exceeded 5% for more than 1 s, the data were excluded due to suspected tracking artifacts. The smoothing was used only for error detection; all subsequent analyses were performed on the unsmoothed data. In addition, we excluded data if the WBA of either wing dropped below 40° for at least 0.5 s, as this indicated a cessation of flight. Finally, entire trials were excluded if the hoverfly was not flying for more than 50% of the trial duration. Head and leg kinematic data were excluded whenever the corresponding WBA data were excluded, ensuring consistent trial inclusion across behavioural metrics.

Visual stimuli

Visual stimuli were generated using custom software (*https://github.com/HoverflyLab/FlyFly/releases/tag/v4.2.3*) written in MATLAB, incorporating the Psychophysics Toolbox[49,50]. All screens had a refresh rate of 165 Hz and a linearized contrast with a mean illuminance of 200 Lux. For intracellular recordings, the hoverfly was placed 13 cm away from a ViewSonic screen with a resolution of 2560 × 1440 pixels, corresponding to 143° × 107° of the visual field. For extracellular recordings, the hoverfly was placed 6.5 cm away from a 2560 × 1440 pixel Asus screen, yielding a projected visual field of 155° × 138° (Supplementary Fig. 6a). For behavioural recordings, the hoverfly was placed 10 cm from a vertically orientated Asus screen (1440 × 2560 pixel, Supplementary Fig. 6b) producing a projected size of 118° × 142°. To evaluate the impact of different screen orientations in electrophysiology and behaviour, visual stimuli were presented either full-screen or using the central 1440 × 1440 pixel square (Supplementary Fig. 6c, d).

Receptive field mapping

To map each neuron's receptive field, we presented local sinusoidal gratings (average 38 × 38°) drifting in 8 directions for 0.36 s each, across 48 overlapping locations, as described in detail previously[14]. Stimuli were full contrast, with an average spatial frequency of 0.14 cycles/° and a temporal frequency of 5 Hz. At each location, we calculated the local maximum spike frequency (red, inset, Fig. 1b, e). After subtracting the spontaneous rate, calculated for 0.8 s preceding stimulus onset (dotted line, inset, Fig. 1b, e), we interpolated the resulting local maximum responses to a ten-fold higher spatial resolution (colour coding, Fig. 1a, d). We then quantified the 50% response maximum using Matlab's *contour* function (black, Fig. 1b, e). We created a polygon-shape of this 50% contour line using Matlab's *polyshape* function to calculate the receptive field size, defined as its width and height (Supplementary Fig. 2f), and used the *centroid* function to identify the centre of this polyshape (red circle, Fig. 1b, e). As recordings were performed with the animal ventral side up (Supplementary Fig. 3a, 6a), receptive fields were rotated to display them with the dorsal visual field up.

Next, at each location, we fit a cosine function to the responses to the different directions of motion, to extract the local preferred direction (LPD) and local motion sensitivity (LMS; inset, Fig. 1c, f). These were visualized as vectors where angle indicates LPD and length indicates LMS (arrows, Fig. 1a, d). We defined the receptive field preferred direction as the median of LPDs at locations where LMS exceeded 50% of the maximum (black and red arrows; Fig. 1c, f), using *circ_median* from the CircStat toolbox for MATLAB[51]. We calculated the LPD variance using the *circ_var* functions from CircStat toolbox for MATLAB[51], of LPDs at locations where LMS exceeded 50% of the maximum (black and red arrows; Fig. 1c, f).

We extracted unpublished receptive field data from 100 reference neurons (other data from five of these optic flow sensitive descending neurons has been published previously[28]) to set exclusion criteria (red shading, Supplementary Fig. 2a, b and c) and to classify the OFS DNs used in the rest of this study. OFS DN1 LHS neurons were defined by receptive field preferred directions between 120° and 200° (light green, Fig. 1g, i). OFS DN1 RHS neurons were defined by receptive field preferred directions between 340° and 60° (dark green, Fig. 1g, i). OFS DN2 neurons were classified by receptive field preferred directions between 220° and 320° (yellow and orange, Fig. 1g, i), with the azimuthal location of the receptive field centre determining whether they were LHS or RHS (yellow and orange, Fig. 1h).

A polar plot where the distance from origo indicates azimuthal position, and the location along the radius the preferred direction, confirms that the LHS and RHS of OFS1 and OFS2 cluster distinctly (Supplementary Fig. 1a). To test whether incorporating additional receptive field parameters would reveal further neuronal subtypes, we performed k-means clustering in Matlab using z-score normalised data. The additional parameters included receptive field centre elevation, receptive field height and width (see Supplementary Fig. 2f), maximum LMS (see Supplementary Fig. 2a), the number of positions with LMS values exceeding 50% of the maximum (see Supplementary Fig. 2b), and LPD variance (see Supplementary Fig. 2c). However, the Callinski-Harabasz[52] values indicate that adding additional receptive field parameters actually reduced clustering performance (Supplementary Fig. 1b). In contrast, clustering based solely on preferred direction and azimuthal location yielded four well-defined groups (Supplementary Fig. 1c), and produced the highest Callinski-Harabasz value (Supplementary Fig. 1b).

Directional sensitivity

Full-screen sinusoidal gratings were presented at full contrast, using the same spatial (0.14 cycles/°) and temporal (5 Hz) frequencies as in receptive field mapping. For each stimulus direction, mean spike frequency was calculated over the 1 s stimulus duration, excluding the first 100 ms to avoid onset transients[53].We fit a cosine function to the responses to the eight different directions of motion, to extract the preferred direction and response amplitude (Supplementary Fig. 3b), and then plotted these values for OFS DN1 (Supplementary Fig. 3c) and DN2 neurons (Supplementary Fig. 3d). To account for the ventral-side-up recording position (Supplementary Fig. 3a) directional

responses were rotated 180° (Supplementary Fig. 3f, g and h). In addition, to display all neurons as RHS, and assuming mirror-symmetry, we flipped LHS neurons across the midline (Supplementary Fig 2i, j, k and l).

Responses to optic flow

We used a starfield stimulus to generate the type of perspective-corrected optic flow that would have been seen by the hoverfly if it was moving through a space of 2 cm diameter spheres (for details, see Ref[14,33]). These simulated translations at 0.5 m/s (sideslip, lift, and thrust) or rotations (pitch, yaw, and roll), at 50°/s. To quantify neural responses, the mean spike frequency was calculated over the 0.97 s stimulus duration, excluding the first 0.1 s to avoid onset-related transients[53]. The spontaneous firing rate, averaged across 0.48 s immediately preceding stimulus onset (open circles, Supplementary Fig 4a, b), was subtracted from the response.

Velocity response functions

We used four types of optic flow: three translations (sideslip, lift and thrust, Supplementary movie 2-7) and one rotation (roll, Supplementary movie 1, 8, 9). Translations were presented at velocities of −2, −1.5, −1, −0.4, −0.2, −0.1, 0, 0.1, 0.2, 0.4, 1, 1.5, and 2 m/s, while rotations were presented at 200, −150, −100, −40, −20, −10, 0, 10, 20, 40, 100, 150, and 200°/s. The sign of the velocity indicates the direction of motion as seen by the fly when corrected for its position, with positive values corresponding to counterclockwise roll, leftward sideslip, downward lift, and thrust moving away. Conversely, negative values indicate clockwise roll, rightward sideslip, upward lift, and thrust moving toward the hoverfly. The upper limit was defined by the movement of the individual dots within the starfield stimulus between frames, i.e. was limited by the refresh rate of the screen.

Each trial consisted of 39 stimuli (13 unique velocities × 3 repetitions), presented in a random order, with each stimulus lasting 2 s, immediately followed by the next velocity. Trials began with a 1 s blank screen, which served as the pre-stimulation baseline (Fig. 3a and Fig. 5c).

Each optic flow condition was repeated multiple times, resulting in at least nine repetitions for each velocity and neuron, and five repetitions for each velocity and animal in behaviour.

For neuronal recordings, velocity response function trials were interleaved with the optic flow stimuli described above. In behavioural experiments, a flight refresher sequence interspersed each velocity tuning trial. This consisted of sinusoidal gratings (200° wavelength, 5 Hz) drifting rightward, leftward, and rightward again for 4 s each.

Neural responses were quantified as the mean spike frequency during the final second of stimulation (grey shaded areas, Fig. 3a–c). We then calculated the median across trials for each velocity (Fig. 3d). Pre-stimulation activity (spontaneous rate) was measured over a 2 s window immediately preceding stimulus onset. Neural responses are displayed after subtracting the response when viewing a stationary stimulus (filled symbols, Supplementary Fig. 4a, b).

In behavioural experiments, we extracted the mean wing beat amplitude of the left and right wings ($\overline{WBA_L}$, $\overline{WBA_R}$, Fig. 5b) during the final second of stimulation (grey shaded areas, in Fig. 5 c, d and e). For each velocity, we calculated the WBA difference (WBAD, defined as $\overline{WBA_L} - \overline{WBA_R}$) and the WBA sum (WBAS, defined as $\overline{WBA_L} + \overline{WBA_R}$, Fig. 5b). We then calculated the median across repetitions for each individual (Fig. 5f). Pre-stimulation responses were averaged over a 0.5 s time window immediately preceding stimulus onset.

WBA responses are displayed after subtracting the response when viewing a stationary stimulus (filled symbols, Supplementary Fig. 4c).

We defined the head angle as the angle between a straight line joining the 2 tracked points on the head (using *polyfit* in matlab, Fig. 7a, b) and the longitudinal axis of the thorax (Fig. 7a, b). As we filmed in one plane only, this measurement can be caused by a combination of head rotations, but seem to be dominated by roll rotations (Supplementary movie 2-9). We measured the distance between the proximal and distal points of the forelegs (Fig. 7a, c).

Note that the forelegs were mostly hidden under the animal from our dorsal view, and could only be seen when extended anteriorly (e.g. Fig. 5a, see also Supplementary movie 2-9). Data are displayed as the mean extension of the left and right foreleg. We measured the distance between the hind leg knee and a lateral point on the mid-abdomen (Fig. 7a, d). Hind leg data are displayed as the mean or the difference of the left and right hind leg. All body parts data are displayed after subtracting the response when viewing a stationary stimulus (filled symbols show hindleg data, Supplementary Fig. 4d).

Response onset

For neuronal recordings, we compared onset times for clockwise roll (+50°/s) and either upwards lift (+0.5 m/s) for OFS DN 1 or downwards lift (-0.5 m/s) for OFS DN2, stimuli which generated strong responses in these neurons (Fig. 3 e, f). Mean spike frequency was calculated over the 0.97 s stimulus duration, excluding the first 0.1 s to avoid onset transients[53]. Onset was defined as the first time point after the first 0.1 s, where spike rate exceeded 80% of the mean.

For behaviour, we used WBA responses to roll (-200°/s) and lift (+2 m/s). Mean WBAS was defined as the average response during the final second of stimulation, and onset was defined as the first time point where WBAS exceeded 80% of this mean. We also quantified WBAS, head, fore-and hind leg onsets to sideslip (+2 m/s). For each body part, we quantified the mean response during the final second of stimulation, and onset was defined as the first time point where the response exceeded 80% of this mean.

Statistics

Throughout the text *n* refers to individual repetitions, whereas *N* refers to individual neurons (electrophysiology) or animals (behaviour). All data are presented as median and interquartile range, unless otherwise indicated.

Statistical analyses were performed in Prism 10.4.0 (GraphPad Software), except for circular statistics, which were conducted using the CircStat toolbox for MATLAB[51]. The results of the statistical tests are given in the text, figure legends and in Table 1 and Table 2. For behavioural data the *p*-values were Bonferroni adjusted[54] for multiple comparisons (Table 2).

Supplementary figures

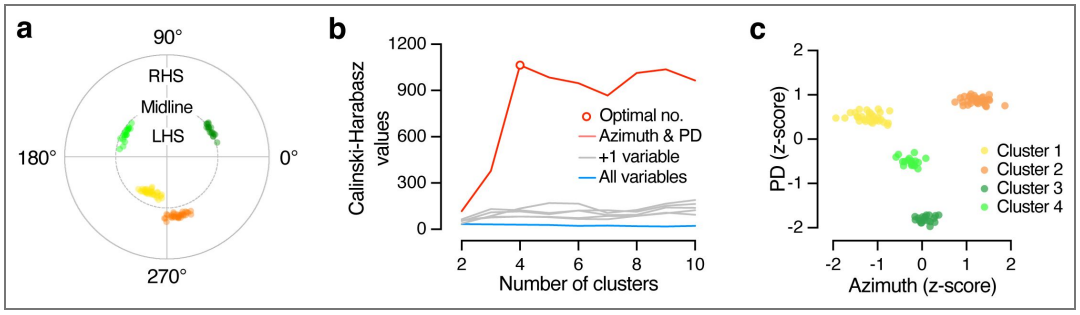

Supplementary Fig 1. **a** The four clusters as identified by us (see Fig. 1g, h and i) displayed on a polar plot where the distance from origo illustrates the azimuthal position and the position along the circumference the preferred direction, colour coded as in the main paper (pale green: OFS DN1 LHS; dark green: OFS DN1 RHS; yellow: OFS DN2 LHS; orange: OFS DN2 RHS). **b** The Calinski-Harabasz value[52] as a function of cluster number when using only the azimuthal location of the receptive field centre and the preferred direction (red), or when adding one other receptive field criterion (grey, receptive field centre elevation, receptive field height or width, maximum LMS, the number of positions with LMS values exceeding 50% of the maximum, or LPD variance, see Methods), or all receptive field criteria (blue). **c** The resulting z-score for azimuthal location and preferred direction, and the four clusters using k-means clustering in Matlab.

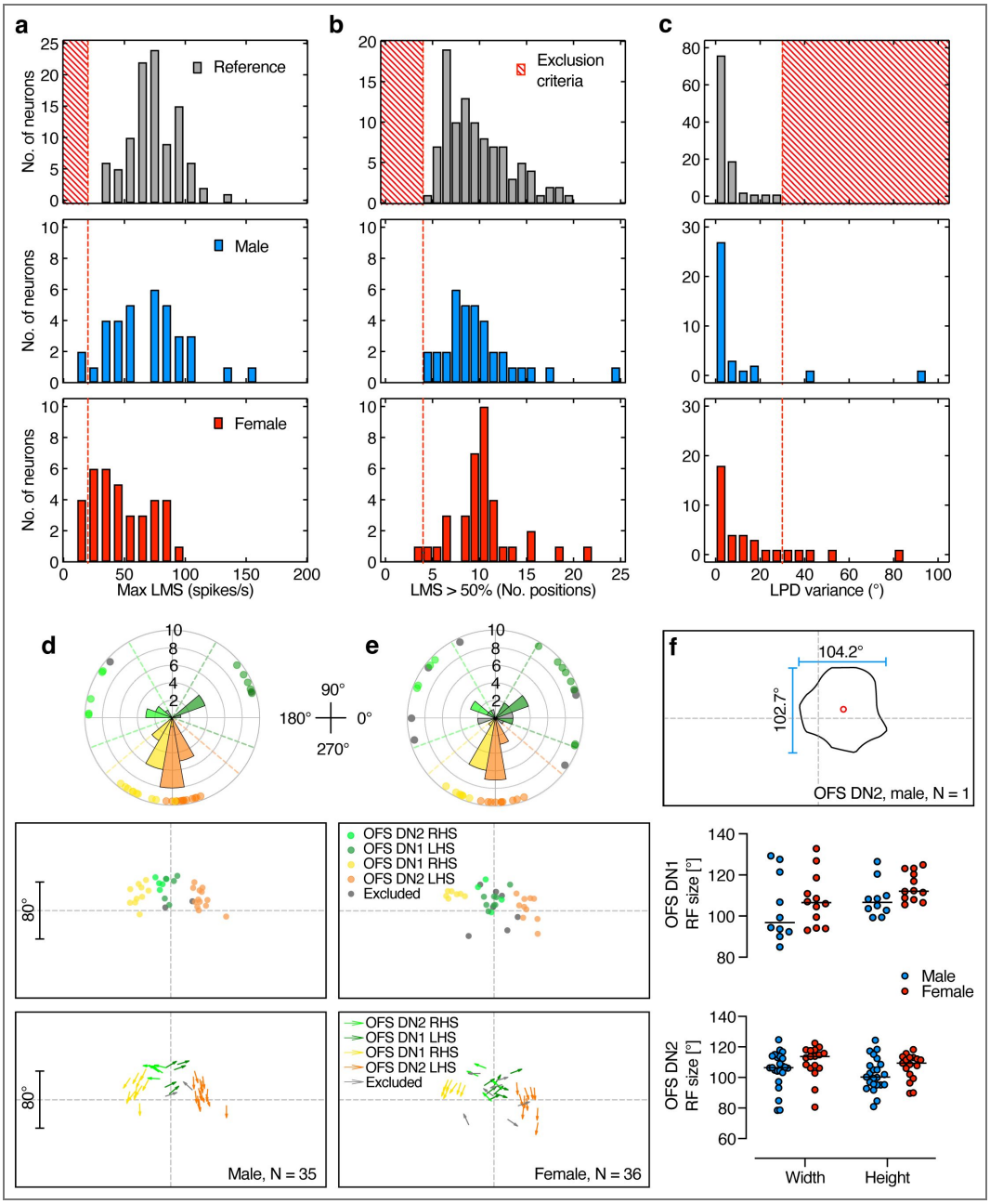

Supplementary Fig 2. Exclusion criteria and receptive field comparisons in male and female OFS DNs.

a Distribution of maximum local motion sensitivity (LMS) in 100 male reference neurons (grey histogram, N = 100) compared to the neurons used for quantification in the rest of the paper (N = 35 males, 36 females). Six neurons with a maximum LMS below 20 spikes/s (red cross-hatched region or dashed line) were excluded from further analysis. **b** Number of stimulus positions with LMS greater than 50% of the neuron's maximum LMS (black and red arrows in Fig. 1c and f). Neurons with fewer than 4 positions were excluded. **c** Distribution of LPD variance. Neurons with directional variance exceeding 30° were excluded. **d** Classification of male neurons based on receptive field centre and preferred direction. The top panel shows the preferred directions across neurons, with dashed lines indicating the directional thresholds used for neuron type classification. The middle panel shows receptive field centre locations, and the bottom panel illustrates the relationship between receptive field centre and the receptive field preferred direction for all 35 male neurons, with 2 neurons excluded from further analysis (grey). Note that the scale is the same for the azimuth and elevation, and the scale bar corresponds to both the x- and y-axis. **e** Same classification criteria applied to 36 female neurons, with 7 neurons excluded (grey). **f** The receptive field width and height at the 50% contour line for the remaining OFS DN 1 (N = 10 males, 12 females) and OFS DN2 (N = 23 males, 17 females). Individual data points from independent neurons, with black lines representing the median.

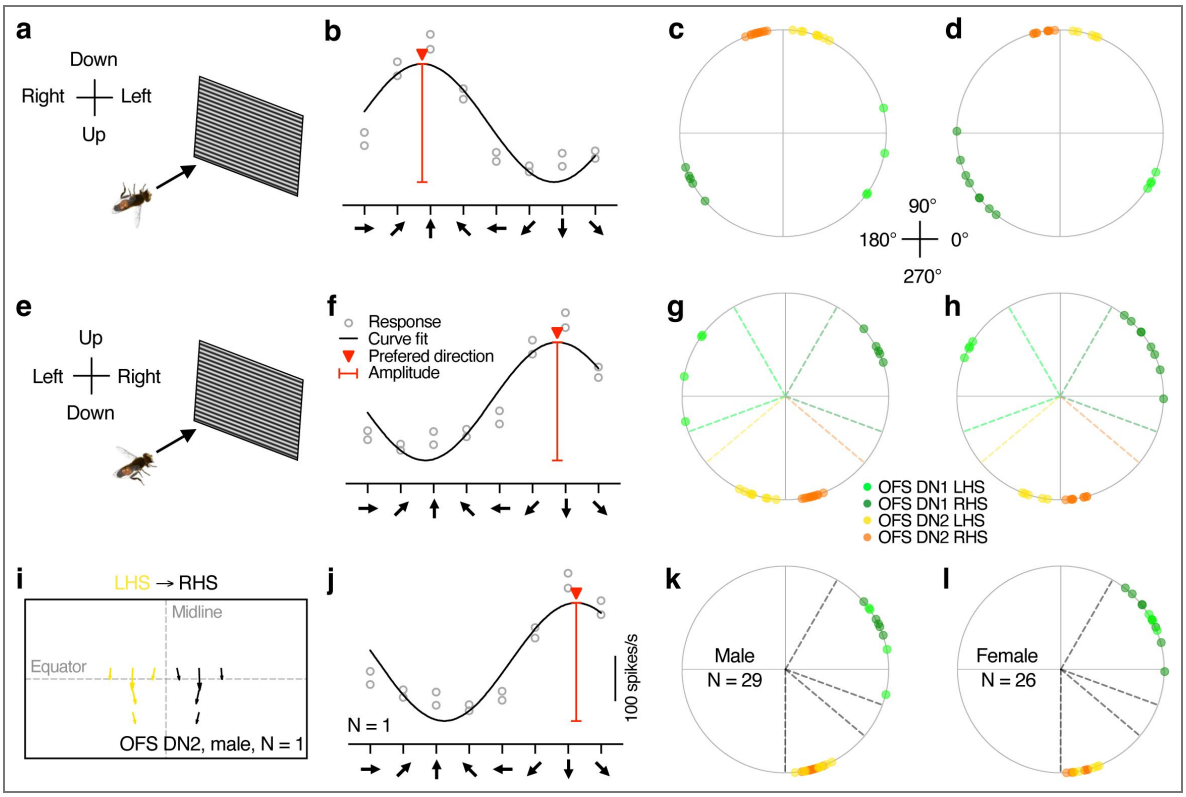

Supplementary Fig 3. Schematic illustration showing the steps used to standardize data across recordings.

a. Top panel, ventral-side-up position of hoverfly during electrophysiology recordings. **b** Response of an example OFS DN2 neuron to a full-screen, full-contrast sinusoidal grating (spatial wavelength 7°; temporal frequency 5 Hz) moving in eight different directions. The red arrowhead shows the neuron's preferred direction, and the red line indicates response amplitude. **c** Preferred direction of male hoverfly OFS DNs (N = 29). Neurons are colour coded by classification. **d** Preferred direction of female hoverfly OFS DNs (N = 26). Neurons are colour coded by classification. **e** We rotated the data 180° to display the dorsal visual field up. **f** Direction sensitivity of the same neuron as in panel b after rotating the data 180°. **g** Preferred direction of male hoverfly OFS DNs after rotating the data 180°. Neurons are colour coded by classification, with dashed lines indicating the receptive field thresholds. **h** Preferred direction of female hoverfly OFS DNs after rotating the data 180°. **i** To display all neural data as RHS neurons, we flipped LHS neurons along the midline (yellow to black). **i** Resulting direction sensitivity after flipping along the midline of the same neuron as in panels b and f. **k** Preferred direction of male hoverfly OFS DNs when displayed as RHS only. **l** Preferred direction of female hoverfly OFS DNs when displayed as RHS only.

Supplementary Fig. 4. Comparison of spontaneous activity and responses to stationary stimuli.

a Spontaneous activity (open shapes) and responses of a male OFS DN1 to the stationary starfield (filled shapes), from data extracting directional sensitivity (as in Fig. 2; circles) or velocity response functions (as in Fig. 3; triangles). **b** Spontaneous activity and responses of OFS DN2, displayed as in panel a. **c** WBAS before stimulus presentation (open squares) or when viewing the stationary starfield (filled squares), quantified during velocity response function experiments (as in Fig. 5). **d** Hind leg extension before stimulus presentation (open diamonds) or when viewing the stationary starfield (filled diamonds), quantified during velocity response function experiments (shown in Fig. 7). The data points show data from individual neurons (a and b) or animals (c and d), with lines representing the median. Asterisks denote statistical significance, two-way ANOVA with uncorrected Fisher's LSD test: * $p < 0.05$, ** $p < 0.01$ and *** $p < 0.001$.

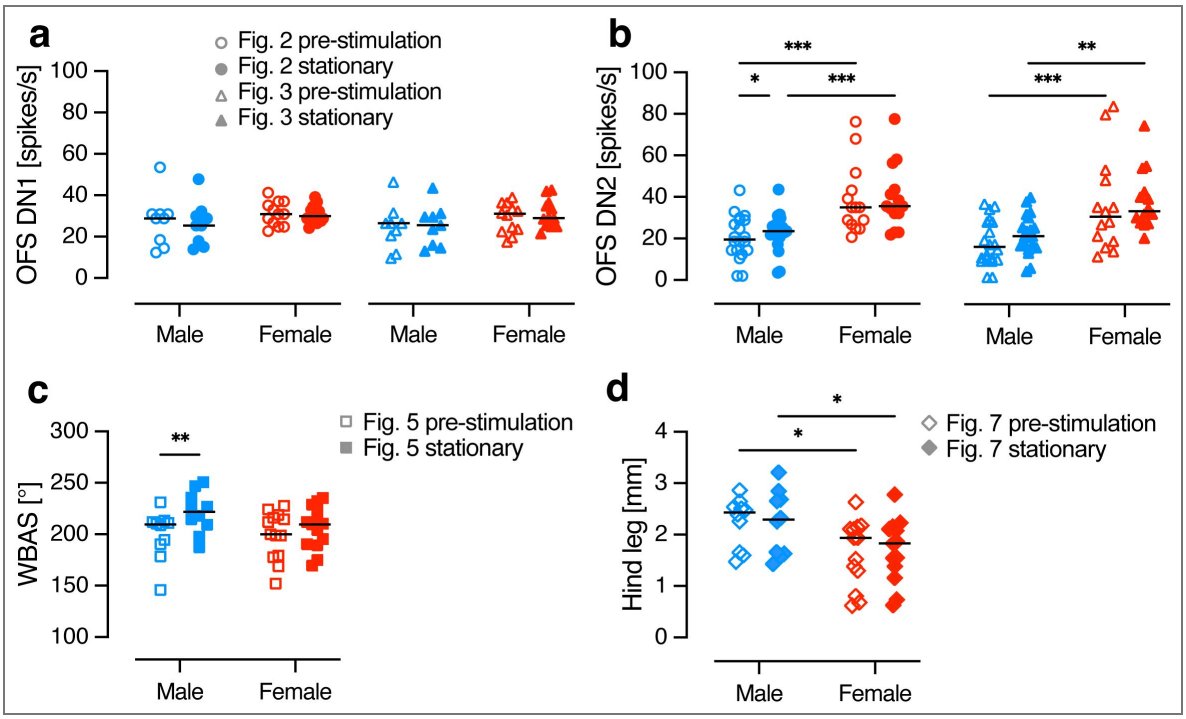

Supplementary Fig 5. Morphological quantification of OFS DN2.

a Schematic diagram of the hoverfly central brain and thoracic ganglia showing locations where the cervical connective (CC) and the OFS DN2 (orange) widths were measured. **b** Width measurements of OFS DN2 axons along the cervical connective at four anatomical landmarks: (1) immediately posterior to the central brain, (2) upper third of the CC, (3) lower third of the CC, and (4) immediately anterior to the thoracic ganglion. Data are shown for 3 male (blue) and 3 female (red) hoverflies. **c** Width of the anterior end of the cervical connective in the same individuals. All data are presented as individual animals with the horizontal lines indicating median.

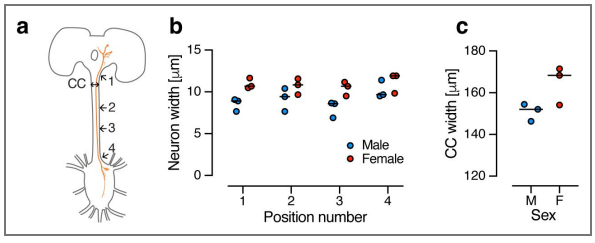

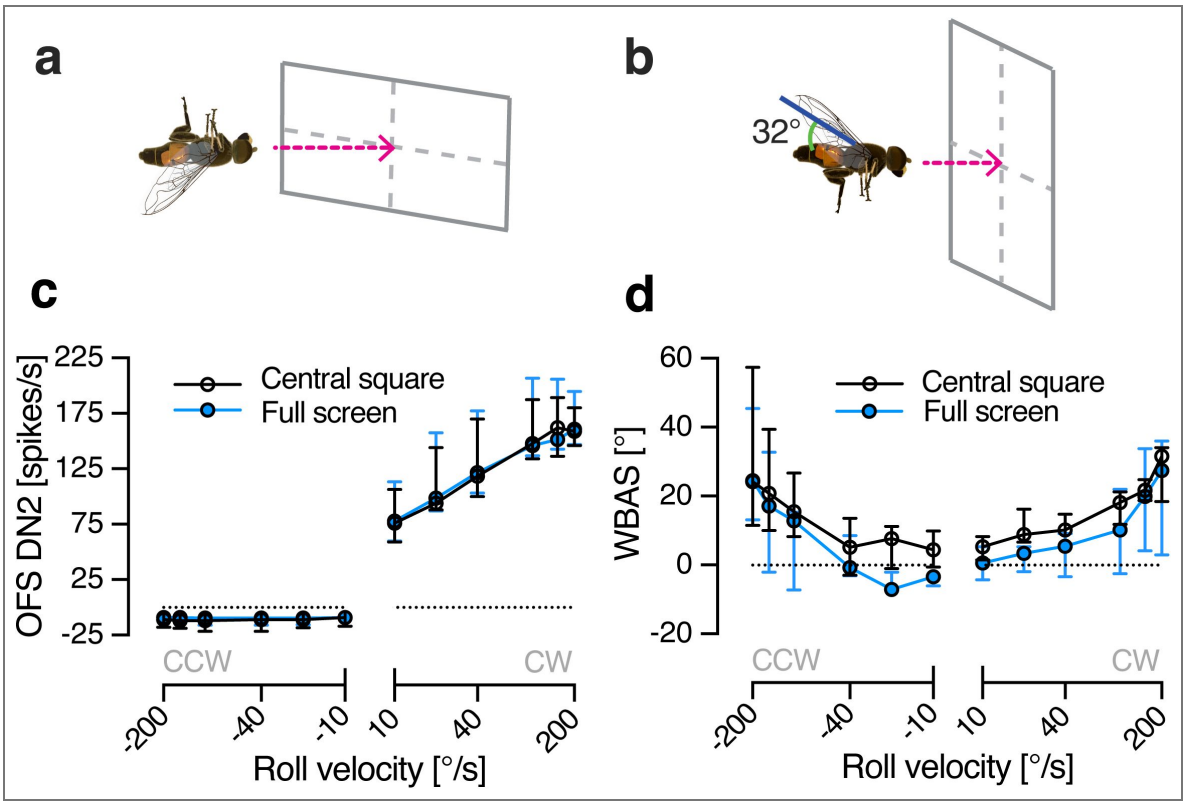

Supplementary Fig 6. Impact of stimulus size on neural and behavioural velocity response functions.

a Electrophysiological recordings were performed with the hoverfly orientated ventral side up, facing the centre of a horizontally oriented visual display. **b** In behavioural experiments, the hoverfly was tethered at 32° angle, parallel to the ground, facing the centre of a vertically aligned visual display. **c** Velocity response functions of male OFS DN2 neurons when the stimulus covered either the full screen (blue) or the central square (black, N = 7). **d** Velocity response functions of WBAS in male hoverflies when the stimulus covered either the full screen (blue) or the central square (black, N = 5). All data are presented as median and interquartile range.

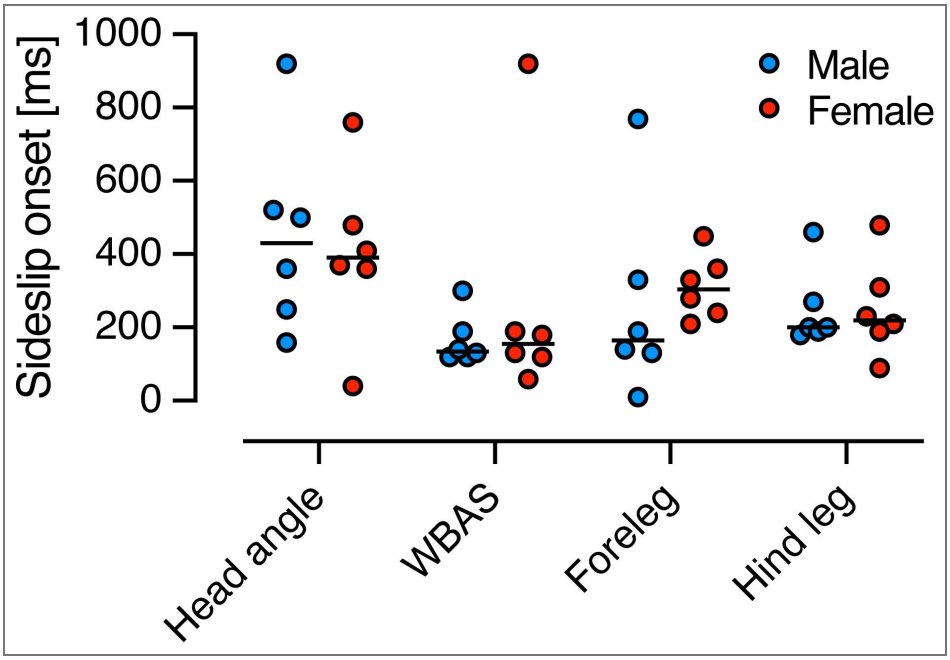

Supplementary Fig 7. Response onset to sideslip.

Onset of head angle, WBAS, fore- and hind legs to sideslip (+2 m/s) in males (N = 6) and females (N = 6). There was no significant difference between body parts, nor males and females (two-way ANOVA, p = 0.08, p = 0.67 and p = 0.84, for body parts, sex and interaction respectively). All data are presented as individual animals with the horizontal lines indicating median.

Data availability

All data and analysis scripts have been submitted to DataDryad (10.5061/dryad.tb2rbp0fd).

Acknowledgements

We thank Biomedical Engineering at SAHLN and the Botanic Gardens of Adelaide for their ongoing support. We thank the editor and the two Reviewers for their feedback which greatly improved our paper. This research was funded by the US Air Force Office of Scientific Research (AFOSR, FA9550-19-1-0294 and FA9550-23-1-0473) and the Australian Research Council (ARC, DP210100740, DP230100006 and DP250104770).

Additional information

CRediT author statement

Sarah Nicholas: conceptualization, methodology, validation, formal analysis, investigation, data curation, writing – original draft, visualization, project administration; **Katja Sporar Klinge:** methodology, validation, formal analysis, investigation, data curation, writing – review and editing, visualization; **Luke Turnbull:** methodology, validation, investigation, writing – review and editing; **Annabel Moran:** investigation, writing – review and editing; **Aika Young**: investigation, writing – review and editing; **Yuri Ogawa:** methodology, validation, formal analysis, investigation, data curation, writing – original draft, visualization, supervision, project administration; **Karin Nordström:** conceptualization, validation, formal analysis, resources, writing – original draft, visualization, supervision, project administration, funding acquisition.

Funding

Funder	Grant reference number	Author
US Air Force of Scientific Research	FA9550-19-1-0294	Karin Nordström
US Air Force of Scientific Research	FA9550-23-1-0473	Karin Nordström Yuri Ogawa
Department of Education and Training | Australian Research Council (ARC)	DP210100740	Karin Nordström
Department of Education and Training | Australian Research Council (ARC)	DP230100006	Karin Nordström
Department of Education and Training | Australian Research Council (ARC)	DP250104770	Yuri Ogawa

Author ORCID iDs

Sarah Nicholas: https://orcid.org/0000-0002-5555-9421
Katja Sporar Klinge: https://orcid.org/0009-0004-7224-6568
Aika Young: https://orcid.org/0009-0000-5028-6164
Yuri Ogawa: https://orcid.org/0000-0002-9708-7063
Karin Nordström: https://orcid.org/0000-0002-6020-6348

Additional files

Supplementary movie 1. Neural response to roll optic flow. The video shows the raw extracellular response of an OFS DN2 in red when the hoverfly was viewing an example roll stimulus, as in Fig. 3 of the main paper.

Supplementary movie 2. Female behavioural response to sideslip optic flow. The video on the left shows a female hoverfly filmed from above, with coloured dots indicating the body parts tracked by DeepLabCut to extract wing beat amplitude (WBA), head angle, and fore- and hind leg

kinematics. The stimulus viewed by the hoverfly is shown on the right, with stimulus velocity indicated above the hoverfly video. The movie relates to Fig. 5 of the main paper.

Supplementary movie 3. Male behavioural response to sideslip optic flow. The video shows a male hoverfly filmed from above, viewing sideslip at different velocities.

Supplementary movie 4. Female behavioural response to lift. A female hoverfly filmed from above, viewing lift optic flow at different velocities.

Supplementary movie 5. Male behavioural response to lift. A male hoverfly filmed from above, viewing lift optic flow at different velocities.

Supplementary movie 6. Female behavioural response to thrust. A female hoverfly filmed from above, viewing thrust optic flow at different velocities.

Supplementary movie 7. Male behavioural response to thrust. A male hoverfly filmed from above, viewing thrust optic flow at different velocities.

Supplementary movie 8. Female behavioural response to roll. A female hoverfly filmed from above, viewing roll optic flow at different velocities.

Supplementary movie 9. Male behavioural response to roll. A male hoverfly filmed from above, viewing roll optic flow at different velocities

References

1 **Mauss A. S.,** Borst A (2020) Optic flow-based course control in insects. *Curr Opin Neurobiol* **60**:21-27 https://doi.org/10.1016/j.conb.2019.10.007 | PubMed

2 **Pierantoni R** (1976) A look into the cock-pit of the fly. The architecture of the lobular plate. *Cell Tissue Res* **171**:101-122 https://doi.org/10.1007/bf00219703 | PubMed

3 **Zhao A.,** et al. (2023) A comprehensive neuroanatomical survey of the *Drosophila* Lobula Plate Tangential Neurons with predictions for their optic flow sensitivity. *bioRxiv* https://doi.org/10.1101/2023.10.16.562634 | PubMed

4 **Franz M. O.,** Krapp H. G (2000) Wide-field, motion-sensitive neurons and matched filters for optic flow fields. *Biol Cybern* **83**:185-197 https://doi.org/10.1007/s004220000163 | PubMed

5 **Krapp H. G.,** Hengstenberg B., Hengstenberg R (1998) Dendritic structure and receptive-field organization of optic flow processing interneurons in the fly. *J Neurophysiol* **79**:1902-1917 https://doi.org/10.1152/jn.1998.79.4.1902 | PubMed

6 **Wei H.,** Kyung H. Y., Kim P. J., Desplan C (2020) The diversity of lobula plate tangential cells (LPTCs) in the Drosophila motion vision system. *Journal of Comparative Physiology A* **206**:139-148 https://doi.org/10.1007/s00359-019-01380-y | PubMed

7 **Strausfeld N. J.,** Bassemir U. K (1985) Lobula plate and ocellar interneurons converge onto a cluster of descending neurons leading to neck and leg neuropil in *Calliphora erythrocephala*. *Cell Tissue Res* **240**:617-640 https://doi.org/10.1007/bf00216351

8 **Strausfeld N. J.,** Seyan H. S (1985) Convergence of visual, haltere, and prosternai inputs at neck motor neurons of *Calliphora erythrocephala*. *Cell and Tissue Research* **240**:601-615 https://doi.org/10.1007/bf00216350

9 **Namiki S.,** Dickinson M. H., Wong A. M., Korff W., Card G. M (2018) The functional organization of descending sensory-motor pathways in *Drosophila*. *eLife* **7**:e34272 https://doi.org/10.7554/eLife.34272 | PubMed

10 **Suver M. P.,** Huda A., Iwasaki N., Safarik S., Dickinson M. H (2016) An Array of Descending Visual Interneurons Encoding Self-Motion in Drosophila. *J Neurosci* **36**:11768-11780 https://doi.org/10.1523/JNEUROSCI.2277-16.2016 | PubMed

11 **Erginkaya M.,** et al. (2023) A competitive disinhibitory network for robust optic flow processing in *Drosophila*. *bioRxiv* https://doi.org/10.1101/2023.08.06.552150

12 **Haikala V.,** Joesch M., Borst A., Mauss A. S (2013) Optogenetic control of fly optomotor responses. *J Neurosci* **33**:13927-13934 https://doi.org/10.1523/jneurosci.0340-13.2013 | PubMed

13 **Pokusaeva V. O.,** Satapathy R., Symonova O., Joesch M (8830) (2024) Bilateral interactions of optic-flow sensitive neurons coordinate course control in flies. *Nat Commun* **15** https://doi.org/10.1038/s41467-024-53173-w | PubMed

14 **Nicholas S.,** Leibbrandt R., Nordström K (2020) Visual motion sensitivity in descending neurons in the hoverfly. *J Comp Physiol A* **206**:149-163 https://doi.org/10.1007/s00359-020-01402-0 | PubMed

15 **Haag J.,** Wertz A., Borst A (2007) Integration of lobula plate output signals by DNOVS1, an identified premotor descending neuron. *J Neurosci* **27**:1992-2000 https://doi.org/10.1523/jneurosci.4393-06.2007 | PubMed

16 **Wertz A.,** Borst A., Haag J (2008) Nonlinear integration of binocular optic flow by DNOVS2, a descending neuron of the fly. *J Neurosci* **28**:3131-3140 https://doi.org/10.1523/jneurosci.5460-07.2008 | PubMed

17 **Collett T. S.,** Land M. F (1975) Visual control of flight behaviour in the hoverfly, *Syritta pipiens* L. *J Comp Physiol A* **99**:1-66 https://doi.org/10.1007/bf01464710

18 **Wellington W.,** Fitzpatrick S (1981) Territoriality in the drone fly, *Eristalis tenax* (Diptera, Syrphidae). *Can Entomol* **113**:695-704 https://doi.org/10.4039/Ent113695-8

19 **Collett T. S.,** Land M. F (1978) How hoverflies compute interception courses. *Journal of comparative physiology* **125**:191-204 https://doi.org/10.1007/BF00656597

20 **Dankova K.,** Nicholas S., Nordstrom K (2023) Temperature during pupal development affects hoverfly developmental time, adult life span, and wing length. *Ecol Evol* **13**:e10516 https://doi.org/10.1002/ece3.10516 | PubMed

21 **Nicholas S.,** Thyselius M., Holden M., Nordström K (2018) Rearing and long-term maintenance of *Eristalis tenax* hoverflies for research studies. *JoVE* e57711 https://doi.org/10.3791/57711 | PubMed

22 **Dudley R** (2002) Mechanisms and implications of animal flight maneuverability. *Integr Comp Biol* **42**:135-140 https://doi.org/10.1093/icb/42.1.135 | PubMed

23 **Straw A. D.,** Warrant E.J., O'Carroll D.C (2006) A 'bright zone' in male hoverfly (*Eristalis tenax*) eyes and associated faster motion detection and increased contrast sensitivity. *J Exp Biol* **209**:4339-4354 https://doi.org/10.1242/jeb.02517 | PubMed

24 **van Hateren J. H.,** Hardie R. C., Rudolph A., Laughlin S. B., Stavenga D. G (1989) The bright zone, a specialized dorsal eye region in the male blowfly *Chrysomyia megacephala*. *J Comp Physiol A* **164**:297-308 https://doi.org/10.1007/bf00612990 | PubMed

25 **Hornstein E. P.,** O'Carroll D. C., Anderson J. C., Laughlin S. B (2000) Sexual dimorphism matches photoreceptor performance to behavioural requirements. *Proc R Soc Lond B Biol Sci* **267**:2111-2117 https://doi.org/10.1098/rspb.2000.1257

26 **Nordström K.,** Barnett P. D., de Miguel Moyer, Brinkworth I. M., O'Carroll R. S. A., C D. (2008) Sexual dimorphism in the hoverfly motion vision pathway. *Curr Biol* **18**:661-667 https://doi.org/10.1016/j.cub.2008.03.061 | PubMed

27 **Barnett P. D.,** Nordström K., O'Carroll D. C (2010) Motion adaptation and the velocity coding of natural scenes. *Curr Biol* **20**:994-999 https://doi.org/10.1016/j.cub.2010.03.072 | PubMed

28 **Nicholas S.,** Nordström K (2021) Facilitation of neural responses to targets moving against optic flow. *Proc Natl Acad Sci U S A* **118** https://doi.org/10.1073/pnas.2024966118 | PubMed

29 **Ghosh A.,** Nicholas S., Nordström K., Nowotny T., Knight J (2025) Understanding the mechanism of facilitation in hoverfly TSDNs. *PLOS Computational Biology* **21**:e1012986 https://doi.org/10.1371/journal.pcbi.1012986 | PubMed

30 **Nicholas S.,** Supple J., Leibbrandt R., Gonzalez-Bellido P. T., Nordström K (2018) Integration of small- and wide-field visual features in Target-Selective Descending Neurons of both predatory and non-predatory dipterans. *J Neurosci* **38**:10725-10733 https://doi.org/10.1523/jneurosci.1695-18.2018 | PubMed

31 **Thyselius M.,** Gonzalez-Bellido P. T., Wardill T. J., Nordstrom K (2018) Visual approach computation in feeding hoverflies. *J Exp Biol* **221** https://doi.org/10.1242/jeb.177162 | PubMed

32 **Thyselius M.,** et al. (2023) Hoverfly (Eristalis tenax) pursuit of artificial targets. *J Exp Biol* **226** https://doi.org/10.1242/jeb.244895 | PubMed

33 **Leibbrandt R.,** Nicholas S., Nordström K (2021) The impulse response of optic flow-sensitive descending neurons to roll m-sequences. *J Exp Biol* **224** https://doi.org/10.1242/jeb.242833 | PubMed

34 **Suver M. P.,** Huda A., Iwasaki N., Safarik S., Dickinson M. H (2016) An array of descending visual interneurons encoding self-motion in *Drosophila*. *J Neurosci* **36** https://doi.org/10.1523/jneurosci.2277-16.2016 | PubMed

35 **Mathis A.,** et al. (2018) DeepLabCut: markerless pose estimation of user-defined body parts with deep learning. *Nat Neurosci* **21**:1281-1289 https://doi.org/10.1038/s41593-018-0209-y | PubMed

36 **Ogawa Y.,** et al. (2025) Combining Unity with machine vision to create low latency, flexible and simple virtual realities. *Methods in Ecology and Evolution* **16**:126-144 https://doi.org/10.1111/2041-210X.14449

37 **Götz K. G** (1968) Flight control in *Drosophila* by visual perception of motion. *Kybernetik* **4**:199-208 https://doi.org/10.1007/bf00272517 | PubMed

38 **Maimon G.,** Straw A. D., Dickinson M. H (2010) Active flight increases the gain of visual motion processing in *Drosophila*. *Nat Neurosci* **13**:393-399 https://doi.org/10.1038/nn.2492 | PubMed

39 **Tammero L. F.,** Frye M. A., Dickinson M. H (2004) Spatial organization of visuomotor reflexes in Drosophila. *J Exp Biol* **207**:113-122 https://doi.org/10.1242/jeb.00724 | PubMed

40 **Ristroph L.,** et al. (2010) Discovering the flight autostabilizer of fruit flies by inducing aerial stumbles. *Proc Natl Acad Sci U S A* **107**:4820-4824 https://doi.org/10.1073/pnas.1000615107 | PubMed

41 **Schnell B.,** Weir P. T., Roth E., Fairhall A. L., Dickinson M. H (2014) Cellular mechanisms for integral feedback in visually guided behavior. *Proc Natl Acad Sci U S A* **111**:5700-5705 https://doi.org/10.1073/pnas.1400698111 | PubMed

42 **Theobald J. C.,** Ringach D. L., Frye M. A (2010) Dynamics of optomotor responses in *Drosophila* to perturbations in optic flow. *J Exp Biol* **213**:1366-1375 https://doi.org/10.1242/jeb.037945 | PubMed

43 **Nicholas S.,** Ogawa Y., Nordström K (2023) Dual receptive fields underlying target and wide-field motion sensitivity in looming-sensitive descending neurons. *eNeuro* **10**:ENEURO.0188-0123.2023 https://doi.org/10.1523/eneuro.0188-23.2023 | PubMed

44 **Kim A. J.,** Fenk L. M., Lyu C., Maimon G (2017) Quantitative Predictions Orchestrate Visual Signaling in Drosophila. *Cell* **168**:280-294.e212, https://doi.org/10.1016/j.cell.2016.12.005 | PubMed

45 **Zanker J. M.** (1990) The Wing Beat of Drosophila-Melanogaster .3. Control. *Philos T R Soc B* **327**:45-64 https://doi.org/10.1098/rstb.1990.0042

46 **Sane S. P** (2003) The aerodynamics of insect flight. *Journal of Experimental Biology* **206**:4191-4208 https://doi.org/10.1242/jeb.00663 | PubMed

47 **Niven J. E.,** Scharlemann J. P. W (2005) Do insect metabolic rates at rest and during flight scale with body mass?. *Biol Letters* **1**:346-349 https://doi.org/10.1098/rsbl.2005.0311 | PubMed

48 **Schneider C. A.,** Rasband W. S., Eliceiri K. W (2012) NIH Image to ImageJ: 25 years of image analysis. *Nat Methods* **9**:671-675 https://doi.org/10.1038/nmeth.2089 | PubMed

49 **Brainard D. H.** (1997) The Psychophysics Toolbox. *Spat Vis* **10**:433-436 https://doi.org/10.1163/156856897x00357 | PubMed

50 **Pelli D. G** (1997) The VideoToolbox software for visual psychophysics: transforming numbers into movies. *Spat Vis* **10**:437-442 https://doi.org/10.1163/156856897x00366 | PubMed

51 **Berens P** (2009) CircStat: A MATLAB toolbox for circular statistics. *Journal of Statistical Software* **31**:1-21 https://doi.org/10.18637/jss.v031.i10

52 **Caliński T.,** Harabasz J (1974) A dendrite method for cluster analysis. *Communications in Statistics* **3**:1-27 https://doi.org/10.1080/03610927408827101

53 **Nicholas S.,** Nordstrom K (2020) Persistent Firing and Adaptation in Optic-Flow-Sensitive Descending Neurons. *Curr Biol* **30**:2739-2748.e2732, https://doi.org/10.1016/j.cub.2020.05.019 | PubMed

54 **Abdi H.,** Salkind N. J. (2007) *Encyclopedia of measurement and statistics* Sage.

55 **Kane G. A.,** Lopes G., Saunders J. L., Mathis A., Mathis M. W (2020) Real-time, low-latency closed-loop feedback using markerless posture tracking. *eLife* **9** https://doi.org/10.7554/eLife.61909 | PubMed

Peer reviews

Reviewer #1 (Public review):

Summary:

Hoverflies are renowned for their striking sexual dimorphism in eye morphology and early visual system physiology, as well as in sexually dimorphic behaviors. Surprisingly, male and female flight behaviors in response to optic flow exhibit only subtle differences. Nicholas et al. investigate the sensorimotor transformation of sexually dimorphic visual information into flight steering commands via descending neurons. Using a combination of intracellular and extracellular recordings, neuroanatomical analysis, and behavioral assays, the authors convincingly demonstrate that descending neurons-particularly at high optic flow velocities-exhibit pronounced sexual dimorphisms, while wing steering responses remain largely monomorphic. The study highlights a very interesting discrepancy between neuronal and behavioral response properties.

More specifically, the authors focused on two types of descending neurons that receive inputs from well-characterized wide-field sensitive tangential cells: OFS DN1 and OFS DN2. Their likely counterparts in Drosophila connect to neck, wing and haltere neuropils. The authors characterized the visual response properties of these two neuronal classes in both male and female hoverflies and identified several interesting differences. They then presented the same set of stimuli, tracked wing beat amplitude and analyzed the sum and the difference of right and left wing beat amplitude as a readout of lift or thrust, and yaw turning, respectively. Behavioral responses showed little to no sexual dimorphism, despite the observed neuronal differences.

Strengths:

I find the question very interesting and the results both convincing and intriguing. A fundamental goal in neuroscience is to link neuronal responses and behavior. The current study highlights that the transformations - even at the level of descending neurons to motoneurons - is complex and less straightforward than one might expect.

Weaknesses:

The authors investigated two types of descending neurons, but it was not clear to me how many other descending neurons are thought to be involved in wing steering responses to wide-field motion. I would suggest providing a more in-depth overview of what is known in hoverflies and Drosophila, since the conclusions drawn from the study would be different if these two types were the only descending neurons involved, as opposed to representing a subset of the neurons conveying visual information to the wing neuropil.

Both neuronal classes have counterparts in Drosophila that also innervate neck motor regions. The authors filled hoverfly DNs in intracellular recordings to characterize their arborization in the ventral nerve cord. In my opinion, these anatomical data could be further exploited and discussed a bit more: is the innervation in hoverflies also consistent with

connecting to the neck and haltere motor regions? Are there any obvious differences and similarities to the Drosophila neurons mentioned by the authors? If the arborization also supports a role in neck movements, the authors could discuss whether they would expect any sexual dimorphism in head movements.

Revision comment:

I thank the authors for their detailed replies to my questions and the additional clarifications and analysis included in the paper. All my concerns have been addressed.

https://doi.org/10.7554/eLife.109795.2.sa2

Reviewer #2 (Public review):

Summary:

Many fly species exhibit male-specific visual behaviors during courtship while little is known about the circuit underlying the dimorphic visuomotor transformations. Nicholas et al focus on two types of visual descending neurons (DNs) in hoverflies, a species in which only males exhibit high-speed pursuit of conspecifics. They combined electrophysiology and behavior analysis to identify these DNs and characterize their response to a variety of visual stimuli in both male and female flies. The results show that the neurons in both sexes have similar receptive fields but exhibit speed-dependent dimorphic responses to different optic flow stimuli.

Strengths:

Hoverflies, though not a common model system, show very interesting dimorphic behaviors and provide a unique and valuable entry point to explore the brain organization behind sexual dimorphism. The findings here are not only interesting on their own right but will also likely inspire those working in other systems, particularly Drosophila.

The authors employed rigorous morphology, electrophysiology, and behavior methods to deliver comprehensive characterization of the neurons in question. The precision of the measurements allowed for identifying a subtle and nuanced neuronal dimorphism and set a standard for future work in this area.

Weaknesses:

I'd like to thank the authors for the revised manuscript, especially the new analyses and figures. Most of my earlier concerns have been satisfactorily addressed by now. Interested readers are kindly referred to the authors' responses for the discussion of the limitations of this work.

https://doi.org/10.7554/eLife.109795.2.sa1

Author response:

The following is the authors' response to the original reviews.

> ***eLife Assessment***
>
> *Hoverflies are known for their sexually dimorphic visual systems and exquisite flight behaviors. This valuable study reports how two types of visual descending neurons differ between males and females in their motion- and speed-dependent responses, yet surprisingly, the behavior they control lacks any sexual dimorphism. The results*

> *convincingly support these findings, which will be of interest for studies of visuomotor transformations and network-level brain organization.*

This statement perfectly recapitulates our findings.

> ***Public Reviews:***
>
> ***Reviewer #1 (Public review):***
>
> *Summary:*
>
> *Hoverflies are known for a striking sexual dimorphism in eye morphology and early visual system physiology. Surprisingly, the male and female flight behaviors show only subtle differences. Nicholas et al. investigate the sensori-motor transformation of sexually dimorphic visual information to flight steering commands via descending neurons. The authors combined intra- and extracellular recordings, neuroanatomy, and behavioral analysis. They convincingly demonstrate that descending neurons show sexual dimorphisms - in particular at high optic flow velocities - while wing steering responses seem relatively monomorphic. The study highlights a very interesting discrepancy between neuronal and behavioral response properties.*

Thank you for this summary. Most of the statement perfectly recapitulates the main findings of our paper. However, we want to emphasize that some hoverfly flight behaviors are strongly sexually dimorphic, especially those related to courtship and mating. Indeed, only male hoverflies pursue targets at high speed, chase away territorial intruders, and pursue females for mating. However, other flight behaviours, such as those related to optomotor responses and flights between flowers when feeding, are not sexually dimorphic. We have amended the Introduction and Discussion to make the difference between flight behaviors more clear. Please see lines 77 and 305 onwards.

> *More specifically, the authors focused on two types of descending neurons that receive inputs from well-characterized wide-field sensitive tangential cells: OFS DN1, which receives inputs from so-called HS cells, and OFS DN2, which receives input from a set of VS cells. Their likely counterparts in Drosophila connect to the neck, wing, and haltere neuropils. The authors characterized the visual response properties of these two neuronal classes in both male and female hoverflies and identified several interesting differences. They then presented the same set of stimuli, tracked wing beat amplitude, and analyzed the sum and the difference of right and left wing beat amplitude as a readout of lift or thrust, and yaw turning, respectively. Behavioral responses showed little to no sexual dimorphism, despite the observed neuronal differences.*

Thank you for this very nice summary of our work. We want to clarify that LPTC input to DN1 and DN2 has not been shown directly in hoverflies using e.g. dye coupling, or dual recordings. Instead, the presumed HS and VS input is inferred from morphological and physiological DN evidence, and comparisons to similar data in *Drosophila* and blowflies. We have amended the Introduction to clarify this. Please see line 64 onwards. The rest of the paragraph perfectly recapitulates the main findings of our paper.

> *Strengths:*
>
> *I find the question very interesting and the results both convincing and intriguing. A fundamental goal in neuroscience is to link neuronal responses and behavior. The current study highlights that the transformations - even at the level of descending neurons to motoneurons - are complex and less straightforward than one might expect.*

Thank you.

> *Weaknesses:*
>
> *The authors investigated two types of descending neurons, but it was not clear to me how many other descending neurons are thought to be involved in wing steering responses to wide-field motion. I would suggest providing a more in-depth overview of what is known about hoverflies and Drosophila, since the conclusions drawn from the study would be different if these two types were the only descending neurons involved, as opposed to representing a subset of the neurons conveying visual information to the wing neuropil.*

This is a great point. There are around 1000 fly descending neurons identified in *Drosophila*, of which many could respond to widefield motion, without being specifically tuned to widefield motion. In *Drosophila*, at least 35 descending neuron types receive input in the part of the brain where the LPTC outputs are located, and at least 29 descending neuron types project to the wing motor neuropil. Thus, it is more than likely that other neurons project visual widefield motion information to the wing neuropil. Furthermore, we only measured wing beat amplitude (WBA) as seen in the horizontal plane, as we were filming from above. As such, other wing angle changes and rotations are not quantified. We have amended our Introduction (see line 53 onwards) and Discussion (see line 320 onwards) to address these important points.

> *Both neuronal classes have counterparts in Drosophila that also innervate neck motor regions. The authors filled the hoverfly DNs in intracellular recordings to characterize their arborization in the ventral nerve cord. In my opinion, these anatomical data could be further exploited and discussed a bit more: is the innervation in hoverflies also consistent with connecting to the neck and haltere motor regions? Are there any obvious differences and similarities to the Drosophila neurons mentioned by the authors? If the arborization also supports a role in neck movements, the authors could discuss whether they would expect any sexual dimorphism in head movements.*

These are all great points. We did not see any clear arborizations to the frontal nerve (FN), where we would expect to find the neck motor neurons (NMNs). In addition, while we did see fine arborizations throughout the length of the thoracic ganglion, we saw no strong outputs projecting directly to the haltere nerve (HN). In the revised version of the MS we have modified figure 4 (morphological characterization) to show a magnification of the thoracic ganglion to clarify this.

There are important differences between the morphology of DN1 and DN2 in hoverflies and DNHS1 and DNOVS2 in *Drosophila*, in terms of their projections in the thoracic ganglion. For example, In *Drosophila* DNOVS2, there are several fine branches along the length of the neuron in the thoracic ganglia. Similarly, we found fine branches in *Eristalis tenax* DN2, however, in addition, we found a wide branch projecting to the area of the thoracic ganglion where the prothoracic and pterothoracic nerves likely get their inputs, which we also found in *Eristalis tenax* OFS DN1 (Figure 4). This suggests that both neurons could contribute to controlling the wings and/or the forelegs (which is why we quantified the WBA). In *Drosophila* DNOVS1, there is a similar fat branch to the prothoracic and pterothoracic nerves, Furthermore, while *Drosophila* DNHS1 and DNOVS2 have different morphology, DN1 and DN2 in *Eristalis* looked similar. We have modified the Results section to make this clear, see line 193 onwards.

In addition, to investigate this further, our revised version of the MS includes analysis of the movement of different body parts (the head angle, fore- and hindleg extension) to investigate this further, and to look for sexual dimorphism. Unfortunately, however, this did not include the halteres, as they cannot be seen well in the videos. The new data can be seen in Figure 7.

> ***Reviewer #2 (Public review):***
>
> *Summary:*
>
> *Many fly species exhibit male-specific visual behaviors during courtship, while little is known about the circuit underlying the dimorphic visuomotor transformations. Nicholas et al focus on two types of visual descending neurons (DNs) in hoverflies, a species in which only males exhibit high-speed pursuit of conspecifics. They combined electrophysiology and behavior analysis to identify these DNs and characterize their response to a variety of visual stimuli in both male and female flies. The results show that the neurons in both sexes have similar receptive fields but exhibit speed-dependent dimorphic responses to different optic flow stimuli.*

This statement perfectly recapitulates the main findings of our paper. As mentioned above, while hoverfly flight behaviors related to courtship and mating are strongly sexually dimorphic, other flight behaviours, such as those related to optomotor responses and flights between flowers when feeding, are not. We have amended the Introduction and Discussion to make the difference between flight behaviors more clear. Please see lines 77 and 305 onwards.

> *Strengths:*
>
> *Hoverflies, though not a common model system, show very interesting dimorphic behaviors and provide a unique and valuable entry point to explore the brain organization behind sexual dimorphism. The findings here are not only interesting on their own right but will also likely inspire those working in other systems, particularly Drosophila.*

Thank you.

> *The authors employed rigorous morphology, electrophysiology, and behavior methods to deliver a comprehensive characterization of the neurons in question. The precision of the measurements allowed for identifying a subtle and nuanced neuronal dimorphism and set a standard for future work in this area.*

Thank you.

> *Weaknesses:*
>
> *Cell-typing using receptive field preferred directions (RFPDs): if I understood correctly, this classification method mostly relies on the LPDs near the center of the receptive field (median within the contour in Fig.1). I have two concerns here. First, this method is great if we are certain there are only two types of visual DNs as described in the manuscript. But how certain is this? Given the importance of vision in flight control, I would expect many DNs that transmit optic flow information to the motor center. I'd also like to point out that there are other lobula plate tangential cells (LPTCs) than HS and VS cells, which are much less studied and could potentially contribute to dimorphic behaviors.*

This is very true, and important. As mentioned above, in *Drosophila* there are 35 descending neuron types with inputs on the dorsal surface of the brain (labelled DNp1-35), suggesting that they could receive input from LPTCs. However, only 3 of these have been shown physiologically and morphologically to receive LPTC input, in blowflies and *Drosophila* (DNHS1, DNOVS1, DNOVS2). Note that in both blowflies and fruitflies DNOVS1 gives graded responses, and no action potentials, meaning that we would not be able to record from it using extracellular electrophysiology.

We previously used clustering techniques to show that in *Eristalis*, we can reliably distinguish two types of optic flow sensitive DNs from extracellular electrophysiological data, based on a range of receptive field parameters, and we think that these correspond to DNHS1 and DNOVS2 in *Drosophila* (Nicholas et al, J Comp Physiol A, 2020, cited in paper). As mentioned above in response to Reviewer 1, this does not mean that there are no other neurons that could respond to widefield optic flow, and which might be involved in the WBA we recorded in the paper. However, the point of this paper was not to conclusively show that there are only two optic flow sensitive descending neurons. The point was to say that there are two quite distinct optic flow sensitive neurons that have similar receptive fields in males and females, while their velocity response functions differ between males and females.

We have modified the Introduction (see lines 53 and 64 onwards) and Discussion to make these important points clear to the Reader, including a mention of the 45-60 LPTCs that exist in the lobula plate, and what their role might be.

> *Second, this method feels somewhat impoverished given the richness of the data. The authors have nicely mapped out the directional tuning for almost the entire visual field. Instead of reducing this measurement to 2 values (center and direction), I was wondering if there is a better method to fully utilize the data at hand to get a better characterization of these DNs. As the authors are aware, local features alone can be ambiguous in characterizing optic flows. What's more, taking into account more global features can be useful for discovering potentially new cell types.*

This is a great point, and we did analyse other receptive field properties in this study (shown in previous supp fig 1). In addition, and as mentioned above, we have published a clustering analysis across receptive field properties of these neurons (Nicholas et al, J Comp Physiol A, 2020, cited in paper). The point that we attempted to make in this paper was that by using two strikingly simple metrics, we can reliably distinguish which of the two neuron types we are recording from simply based on azimuthal location and overall directional preference. This makes automated analysis very straightforward. Indeed, we now use this routinely to ID what neuron we are recording from computationally, rather than making a human-based assumption.

However, we agree that this needs to be shown, and that further in depth analysis was warranted. Therefore, we have provided additional receptive field analysis and clustering (see new supplementary figure 1) and associated text. We also want to highlight that all data is uploaded to Data Dryad for anyone interested in doing additional in-depth analyses.

> *Line 131, it wasn't clear to me why full-screen stimuli were used for comparison here, instead of the full receptive field maps. Male flies exhibit sexual dimorphic behaviors only during courtship, which would suggest that small-sized visual stimuli (mimicking an intruder or female conspecific) would be better suited to elicit dimorphic neuronal responses. A similar comment applies to the later results as well. Based on the receptive field mapping in Figure 1, I'm under the impression that these 2 DN types are more suited to detect wide-field optic flows, those induced by self-motion as mentioned in the manuscript. The results are still very interesting, but it's good to make this point clear early on to help set appropriate expectations. Conversely, this would also suggest that there are other visual DN types that are responsible for the courtship-related sexually dimorphic behaviors.*

Thank you for mentioning these important points. Our reasoning for using full-screen stimuli for the analysis on line 131 was that since we used the small sinusoidal gratings for mapping the receptive fields, and to subsequently classify the neurons, it would be unfair to use the same data to investigate potential sexual dimorphism. I.e., we selected neurons that fulfilled certain criteria, and then we cannot rightfully use the same criteria to determine differences.

This was not explicitly mentioned in the paper, so we have modified the text to make this clear to the Reader, see lines 142 onwards.

However, in Supp Figure 2d/e we show that there are no striking receptive field differences between males and females in terms of receptive field center nor directional preference. In Supp Figure 2f we also show that there is no difference between male and female receptive field height and width. We have modified the text to draw the Reader's attention to this figure, and also mention the additional analysis done in response to the comment above.

As a side note, I personally expected at least DN1 to have a smaller receptive field in males, as the hoverfly HSN is strikingly sexually dimorphic (Nordström et al, Curr Biol 2008). However, while optic flow sensitive DNs do respond to small objects (see e.g. the J Comp Physiol paper mentioned above) we did not detect any obvious sexual dimorphism in receptive field properties. Indeed, we think that a different subset of DNs control parts of target pursuit behavior (target selective DNs (TSDNs)). This is now addressed in the modified version of the paper, see line 89-92.

> ***Recommendations for the authors:***
>
> ***Reviewer #1 (Recommendations for the authors):***
>
> *(1) I think that the additional measurement of head turns in response to some of the stimuli that showed the strongest sexual dimorphism would be very interesting, but I fully acknowledge that this might be beyond the scope of the current paper or technically too challenging, requiring additional cameras and a whole new tracking software, etc.*

We have added an additional figure to the paper, with associated text, showing the response of the head, fore- and hindlegs to the same stimuli, as far as we could extract them with only one camera filming from above. The new data can be found in the new figure 7, and associated text.

> *(2) Are the onset measurements for WBD comparable across flight manoeuvres, given that they are limited to a single projection plane?*

This is a great point, and we have now added this caveat in the text, see line 261-262.

> *(3) Line 62 - typo: DNp15 not NDp15.*

Thank you, fixed.

> ***Reviewer #2 (Recommendations for the authors):***
>
> *(1) Related to a comment earlier, in the Introduction, it is mentioned that there are 3 optic flow-sensitive DNs in Drosophila and blowfly. However, I don't see convincing evidence for this in the cited references, none of which have exclusively surveyed all the DNs.*

We have revised this to say that 3 neuron have been identified morphologically and physiologically, but that does not mean that there are no others. Please see line 60 onwards.

> *(2) Line 142 and Supplementary Figure 3, this is stated in the next section, but I think it's better to make it clear that DN2 in females has a higher spontaneous rate before mentioning the starfield. Please also specify if the stationary starfield affects the DN2 rate at all in the female flies.*

Great points. We now describe the spontaneous rate before mentioning the responses to moving starfield stimuli, and highlight that there is no difference between no stimulus (pre-stimulation) and a stationary stimulus. Please see lines 155 onwards.

> *(3) Line 34, 'redress' should be 'to address'.*

Thank you, fixed.

> *(4) Line 59, a bit unclear to me what this sentence is trying to say. Also, I wouldn't say LPTCs are 'indirect' in the sensorimotor transformation -- it's a necessary link in this pathway, no?*

That was indeed a strange sentence. We have simplified it to the following: “LPTCs project to the inferior posterior slope[6], where they synapse with descending neurons[7,8]. In *Drosophila* at least 35 descending neuron types have their inputs in the posterior surface of the brain (named DNp1-35) [9].”

> *(5) Figures:*
>
> *This is a formatting problem. The figure legends are separated from the figures, and there are no titles on the figures to indicate which one is which.*

We are sorry about this. We have added labels to the figures.

> *Figure 1: What kind of geographic projections are these? The azimuth axis is not labeled.*

These stimuli were not perspective corrected, and therefore the RF maps simply reflect the visual monitor. We have clarified this in the figure legend, including mentioning that the axis label is the same for elevation and azimuth.

> *Figure 2a: The error bars are not aligned to the angular axis.*

These have now been aligned.

> *Supplement Figure 2b: I'm not sure why there are two measurements at each stimulus orientation. The bottom panel is confusing -- what do you mean by 'receptive field location'? And what does this red arrow/line mean in the bottom panel?*

Thank you for pointing this out. The figure was supposed to help the reader understand our transformations, so it’s great to know that it needed further explanation. To address this, we have added extra text and panel labels, please see lines 520 onwards.

> *(6) Methods:*
>
> *Line 356: Maybe a picture or schematic drawing would be helpful to explain the setup. For instance, it's unclear what 32 degrees here refers to.*

This is a great suggestion, and a pictogram explaining the set-up can now be seen in Supplementary Fig. 6b.

> *Line 404: What does it mean that 'spatially interpolate 10 times'?*

This sentence has been changed to “After subtracting the spontaneous rate, calculated for 0.8 s preceding stimulus onset (dotted line, inset, Fig. 1b, e), we interpolated the resulting local maximum responses to a ten-fold higher spatial resolution (colour coding, Fig. 1a, d).”

> *Line 405: How to determine the center from the 50% contour?*

We have modified the Methods to explain how this was done, please see lines 478 onwards.

> *Line 408: Please explain more explicitly how LPD and LMS are computed.*

We have modified the Methods to explain how this was done, please see lines 488 onwards.

> *Line 418: Is reference 42 correct? I could be wrong, but this reference seems to be talking about target-selective DNs rather than optic flow-sensitive DNs?*

Yes, this reference is correct. In a supp figure to ref 42, we show data from optic flow sensitive neurons, but not their receptive fields. Thanks for checking.

> *Line 426: Are the full-screen stimuli presented in 8 directions too? Do I understand correctly that the preferred direction vector for the full-screen stimuli is extracted from a cosine fit, which is slightly different from the 'receptive field preferred direction' in the receptive field mapping measurement, which is the median of all the 'local preferred direction' (which are from the cosine fit)?*

We have modified the text to make this clear, please see lines 519 onwards, as well as the receptive field analysis, please see lines 474 onwards.

https://doi.org/10.7554/eLife.109795.2.sa0